Monthly Notices
of the
ROYAL ASTRONOMICAL SOCIETY

Mon. Not. R. Astron. Soc. **407,** 2305–2327 (2010) doi:10.1111/j.1365-2966.2010.16851.x

Numerical models of collisions between core-collapse supernovae and circumstellar shells

Allard Jan van Marle,[1,2⋆] Nathan Smith,[3] Stanley P. Owocki[2] and Bob van Veelen[4]

[1]*Centre for Plasma Astrophysics, K.U. Leuven, Celestijnenlaan 200B, B-3001 Leuven, Belgium*
[2]*Bartol Research Institute, University of Delaware, Newark, DE 19716, USA*
[3]*Astronomy Department, University of California, 601 Campbell Hall, Berkeley, CA 94720, USA*
[4]*Astronomical Institute, Utrecht University, PO Box 80 000, 3508 TA Utrecht, the Netherlands*

Accepted 2010 April 13. Received 2010 March 24; in original form 2009 September 4

ABSTRACT

Recent observations of luminous Type IIn supernovae (SNe) provide compelling evidence that massive circumstellar shells surround their progenitors. In this paper we investigate how the properties of such shells influence the SN light curve by conducting numerical simulations of the interaction between an expanding SN and a circumstellar shell ejected a few years prior to core collapse. Our parameter study explores how the emergent luminosity depends on a range of circumstellar shell masses, velocities, geometries and wind mass-loss rates, as well as variations in the SN mass and energy. We find that the shell mass is the most important parameter, in the sense that higher shell masses (or higher ratios of $M_{\rm shell}/M_{\rm SN}$) lead to higher peak luminosities and higher efficiencies in converting shock energy into visual light. Lower mass shells can also cause high peak luminosities if the shell is slow or if the SN ejecta are very fast, but only for a short time. Sustaining a high luminosity for durations of more than 100 d requires massive circumstellar shells of the order of 10 $M_\odot$ or more. This reaffirms previous comparisons between pre-SN shells and shells produced by giant eruptions of luminous blue variables (LBVs), although the physical mechanism responsible for these outbursts remains uncertain. The light-curve shape and observed shell velocity can help diagnose the approximate size and density of the circumstellar shell, and it may be possible to distinguish between spherical and bipolar shells with multi-wavelength light curves. These models are merely illustrative. One can, of course, achieve even higher luminosities and longer duration light curves from interaction by increasing the explosion energy and shell mass beyond values adopted here.

Key words: hydrodynamics – methods: numerical – stars: mass-loss – supernovae: general – stars: winds, outflows – ISM: supernova remnants.

1 INTRODUCTION

The luminosity of a supernova (SN) results from energy input by a combination of radioactive decay and shock kinetic energy (see e.g. Arnett 1996), and for a Type II SN, the shape of the light curve depends on quantities like the star's initial radius, ejecta mass and explosion energy (Arnett 1996; Young 2004; Kasen & Woosley 2009). For SNe with small initial radii, like SNe of Types Ia, Ib, Ic and peculiar SNe II like SN 1987A that result from blue supergiants, most of the shock-deposited thermal energy imparted to the stellar envelope is converted back into kinetic energy through adiabatic expansion, so nearly all of the observed luminosity comes from the radioactive decay of ^{56}Ni and ^{56}Co. In 'normal' SNe II-P that result from the explosions of red supergiants (RSGs), however, the large initial radius allows some modest fraction (typically 1–2 per cent) of the shock-deposited thermal energy to be radiated away, powering much of the plateau of the light curve, although the vast majority still goes into expansion energy. At late times, even SNe II-P have their luminosity powered by radioactive decay (e.g. Hamuy 2003).

Subsequently, however, as the fast SN ejecta expand, they can collide with dense circumstellar or interstellar medium (CSM/ISM) that may surround the SN. As a result, additional kinetic energy may be transformed once again back into thermal energy through shock heating, which in turn may be lost by radiative cooling if a dense radiative shock forms (e.g. Chevalier & Fransson 2008). This can enhance the luminosity for long after the explosion: some SNe remain radio luminous for decades (Van Dyk et al. 1993; Montes et al. 1998; Williams et al. 2002), and this interaction may power a visible supernova remnant (SNR) such as Cas A for hundreds of

⋆E-mail: allardjan.vanmarle@wis.kuleuven.be

years (Chevalier 1977; Chevalier & Oishi 2003). On the other hand, if the collision with dense CSM happens immediately after the explosion, it may significantly alter the spectrum and light curve of the SN itself. This latter scenario is generally thought to be the case for the observed sub-class of Type IIn SNe (Schlegel 1990; Filippenko 1997), where the 'n' corresponds to 'narrow' or intermediate-width H lines from the shock-heated CSM gas or decelerated SN ejecta (e.g. Chugai & Danziger 1994; Chugai 2001).

In a normal SN, the expected results of radiative cooling and reheating of the SN ejecta due to radioactive decay yield can be estimated from analytical models of stellar structure and explosion physics (Matzner & McKee 1999). In SNe with strong CSM interaction such as the observed class of Type IIn SNe, however, the effects of collisions between an expanding SN and its circumstellar gas are harder to predict with *ab initio* calculations. They depend highly on the density and morphology of the CSM, which in turn depend on the unknown mass-loss behaviour of the star in the few years prior to core collapse – potentially different for each object. A wide variety of CSM environments are possible, leading to a wide diversity of observed light curves and spectral properties.

Recent observations of luminous Type IIn SNe such as SN 2006gy (Smith et al. 2007; Ofek et al. 2007) and SN 2006tf (Smith et al. 2008a) have stretched the boundaries of our understanding of SNe IIn. Their extreme luminosities yield strong evidence that the progenitors of these SNe were surrounded by massive shells, presumably ejected in precursor eruptions during the final years of stellar evolution (Smith et al. 2007, 2008a, 2010; Smith & McCray 2007; Woosley, Blinnikov & Heger 2007). Smith et al. (2007) pointed out that the physical properties (mass, speed, H composition) of these mass ejections were analogous to those observed for giant eruptions of luminous blue variables (LBVs), and especially reminiscent of the giant 1843 eruption of η Carinae (Smith et al. 2003). As the SN ejecta expand, they collide with the recently ejected CSM shell and this collision significantly decelerates the SN expansion, transforming kinetic energy back into thermal energy at the collision front, producing a brilliant fireworks display. The remarkably high luminosity and long duration of the observed emission from SNe 2006gy and 2006tf imply that the circumstellar shells were very massive – of the order of 10–20 $M_\odot$ – in order to sufficiently decelerate the SN blast wave and tap into its available reservoir of kinetic energy (Smith et al. 2007, 2008a, 2010; Smith & McCray 2007; Woosley et al. 2007).

Smith & McCray (2007) have argued based on a simplified analytical model, similar to that of Falk & Arnett (1977), that the high luminosity and long duration of these SNe can be explained by an SN colliding with a very massive and initially opaque CSM shell. We explore this idea here in more detail with a variety of possible CSM environments using numerical simulations. We suggest that the presence and shape of circumstellar shells can be a powerful tool to constrain the evolution of the progenitors of Type IIn SNe. We investigate how the mass, speed and morphology of such shells can influence the evolution of an SN light curve. We undertake a parameter study of SNe with different masses interacting with a selection of possible circumstellar shells, both spherical and bipolar. From these simulations we calculate thermal emission profiles and compare them in order to constrain how the physical properties of circumstellar nebulae can influence the SN light curve, and to constrain the efficiency of converting kinetic energy to light.

Our calculations are simplified in the way we treat the cooling of and radiation from the shocked gas, which we approximate as optically thin radiative cooling; by necessity, our application of these results is therefore limited in scope. An important point to note is that our approach is to simulate a variety of hypothetical SNe to demonstrate *trends* in how the light curve responds to changes in SN and shell properties. We are not attempting a quantitative fit to the observed data for any individual SN. This has been pursued for a few relatively nearby and well-observed SNe IIn, such as SN 1988Z (Turatto et al. 1993; Chugai & Danziger 1994; Aretxaga et al. 1999), SN 1994W (Chugai et al. 2004) and SN 1998S (Chugai 2001), where the CSM properties were derived from fitting the observed light curves and spectra. Those authors inferred massive precursor shell ejections in the few years before core collapse, although the energy demands and required shell masses for these were not as extreme as for SNe 2006tf and 2006gy. Our work here builds upon these earlier studies.

We explain our adopted initial conditions and the numerical method in Sections 2 and 3, respectively, and in Section 4 we discuss some details of the shock interaction. In Section 5 we discuss how the resulting light curves depend on various parameters and in Section 6 we discuss shell velocities, and how these may help to interpret observations. Finally, in Section 7 we interpret our results in context with the most luminous SNe IIn, and in Section 8 we provide a summary.

We include electronic data files containing the results of our simulations with this paper. The L_....dat files contain the total luminosity (erg s^{-1}) as a function of time (s). The V_....dat files contain both the volume- and mass-averaged velocity of the shocked gas (cm s^{-1}) as a function of time (s). A small sample of these tables is provided in Appendices A and B.

2 INITIAL CONDITIONS

2.1 Supernova model

In our simulations, we begin with a core-collapse SN in free expansion as described by Chevalier & Fransson (1992), Matzner & McKee (1999) and Chevalier (2005), which gives a density profile divided in two segments: the inner part has $\rho \sim r^{-m}$, the outer part $\rho \sim r^{-b}$, with $m = 1.06$ and $b = 11.7$ for a progenitor star that still has a large hydrogen envelope at the moment of core collapse. The division between the two power laws lies at the transition velocity:

$$v_{\rm tr} = 3160 \sqrt{\left(\frac{(5-m)(b-5)}{(3-m)(b-3)}\right)} \times \sqrt{E_{51}\left(\frac{10\,{\rm M}_\odot}{M_{\rm ej}}\right)}\ ({\rm km\,s^{-1}}), \quad (1)$$

(Chevalier & Fransson 1992; Chevalier 2005). Using this profile we construct three SNe, with different mass but equal energy. Because of the large value of b, the density drops very quickly at higher velocities. As a result, only a small fraction of the mass is moving fast, limiting the inertia. Therefore, the gas will slow down quickly when it collides with the CSM. Our standard massive-star SN has 30 $M_\odot$ of ejecta mass and 10^{51} erg of total kinetic energy, although we explored a range of SN ejection masses at 6, 10, 30 and 60 $M_\odot$, with total kinetic energies of 0.5, 1 and 2 $\times$ 10^{51} erg. We start each simulation of the CSM interaction at the moment where the SN has expanded to 1 au. Typical maximum velocity for the initial SN is about 30 000 km s^{-1}. However, at this velocity the density is very low and the maximum velocity is quickly reduced to about 10 000 km s^{-1} by the collision with the surrounding medium,

once the simulation begins. The distance it must travel to collide with the shell depends on the shell parameters (see Section 2.2).

Our simulations do not include the effect of photoionization, nor do we take into account the effect of energy injection from radioactive decay. Our calculations simulate only the expected luminosity generated by the SN–CSM interaction shock front; our simulated light curves do not include emission from the expanding SN photosphere powered by diffusion of shock-deposited energy or from radioactive decay. These may affect the light curve at lower CSM-interaction luminosities or very early times before the shock overtakes much of the CSM shell. Note also that our SN model is strictly spherical. Non-spherical SN ejecta outflows would greatly increase the parameter space and require a more complex calculation.

2.2 Circumstellar shell model

For the circumstellar shells, we take a variety of shell properties, but we focus on models reminiscent of the environment of η Carinae (Smith et al. 2003; Smith 2006), as such CSM properties have been proposed for some luminous SN IIn. Namely, we adopt a stellar wind with high mass-loss rate (10^{-5} to $10^{-3}\,M_{\odot}\,yr^{-1}$) and moderate velocity (a few hundred km s^{-1}) for the steady wind phase before and after shell ejection, plus an expanding shell with extremely high density that was ejected in an intermittent outburst reminiscent of giant LBV eruptions, occurring a few years before the SN. The mass-loss rate and velocity of the wind before and after the shell ejection are assumed to be identical. The SN will therefore first encounter a (relatively) low-density wind, then a short stretch of high-density material and then once again the low-density wind after it escapes the shell. We explore a large parameter space, covering a wide range of possible shell masses, velocities, wind mass-loss rates and ages.

We also investigate the effect of a bipolar shell, such as might be ejected by a rapidly rotating star (e.g. Dwarkadas & Owocki 2002; Owocki 2005; Smith & Townsend 2007). The bipolar shape follows the gravitational darkening model for the wind of a rotating star as described by Dwarkadas & Owocki (2002):

$$\frac{\dot{M}(\theta)}{\dot{M}(0)} = 1 - \Omega^2 \sin^2(\theta), \tag{2}$$

$$\frac{v_{\infty}(\theta)}{v_{\infty}(0)} = \sqrt{1 - \Omega^2 \sin^2(\theta)}, \tag{3}$$

with $\Omega \equiv \omega/\omega_{\rm c}$, $\omega = \sqrt{g/R}$ the rotational angular velocity of the star and $\omega_{\rm c}$ the Keplerian angular velocity. Observations have shown that the bipolar shell of η Carinae, for example, follows this shape (Smith 2006). The latitudinal angle θ equals zero at the pole and 90° at the equator. Note that this set of equations only applies for radiatively driven winds. Should the star approach critical rotation during an eruption, mass could be focused to the equator, forming a flattened equatorial structure as well (Smith & Townsend 2007). This is not accounted for in these equations.

The total range of parameters in our simulations is listed in Table 1. In all cases we assume that the shell ejection lasted 2 years, though we explore the effect of different shell cross-sections by varying the velocity. Wind velocity and shell velocity are assumed to be the same, allowing us to use an analytical description, rather than a numerical model, for the shell morphology.

The second to last column in Table 1 gives the efficiency of converting shock kinetic energy into radiated luminosity as found in our simulations, based on the input kinetic energy and the integrated luminosity in the light curve. This is the maximum efficiency corresponding to the bolometric luminosity output. The efficiency in converting shock kinetic energy to *visual* light must be comparable to or less than this value.

Finally, Table 1 shows the velocity of the SN remnant after it has collided with the shell. We measure this velocity at a fixed point in time, except where indicated otherwise; these exceptions are necessary due to the nature of the CSM, which may require a longer time interval before the SN has broken through the shell. Also, we do not list a final velocity for those SNe that interact with bipolar shells, since for these simulations the velocity is angle-dependent.

3 NUMERICAL METHOD

We use the ZEUS 3D code (Stone & Norman 1992; Clark 1996) for our simulations. The grid is spherical and 2D, with 500 gridcells along the radial axis and 100 gridcells along the azimuthal axis, covering a 90° angle from pole to equator. We have seeded both the initial SN and the circumstellar nebula with small-scale density fluctuations (5 per cent for the SN ejecta and 1 per cent for the CSM). This ensures that the SN breaks up the circumstellar shell upon collision.

3.1 Grid evolution

In order to achieve a high resolution at the collision between SN and CSM, the size of the radial gridcells decreases with the radius. This gives us the highest resolution at the outer boundary. Since we need to maintain this high resolution at the collision front, we use the moving grid option that is part of the ZEUS 3D code (see Whalen et al. 2008; van Veelen et al. 2009). At the start of the simulation the freely expanding SN fills the entire grid, with the exception of the outer radial boundary, which is set to an inflow boundary condition with the parameters of the CSM that the SN is running into. At the end of each time-step the code finds the highest radial velocity within 50 radial gridcells of the outer boundary. Using the velocity in this cell as a basis all gridcells are moved outward as well, with velocities

$$v_{\rm grid}[i] = 2v[ic]\frac{r[i] - r[0]}{r[ic] - r[0]}, \tag{4}$$

with $r[i]$ the radius of the gridcell with index i, which runs from 0 to 500, ic the index of the gridcell in which the radial velocity is the highest and $v[ic]$ the highest radial velocity within 50 gridcells of the outer boundary. The physical conditions at the outer boundary are updated each time the grid expands to conform to the values of the CSM at that particular radius. In this way the entire grid is stretched in the radial direction, ensuring that (a) the SNR can never overrun the outer boundary; (b) a high resolution is always maintained close to the outer boundary where the collision takes place and (c) the inner boundary is fixed and does not move. (N.B. This method works well as long as one has to deal with a strong shock. It is not recommended for subsonic expansion).

A drawback of this method is that the circumstellar nebula is supposed to be static during the SN expansion, whereas speeds of the pre-shock CSM for luminous SNe IIn seen in narrow P Cygni absorption features tend to be of the order of 100–500 km s^{-1} (Smith et al. 2007, 2008a, 2010; Trundle et al. 2008). (The CSM speeds listed in Table 1 essentially determine the radii of the shells and therefore their density for an assumed total mass.) However, the velocities of the SN ejecta expansion are much faster than those in the CSM nebula, such that any evolution of the nebula during

Table 1. Simulation input parameters.

Name	M_{sn} ($M_\odot$)	E_{sn} (10^{51} erg)	M_{shell} ($M_\odot$)	$V(\theta = 0)$ (km s^{-1})	$\dot{M}_{wind}$ ($M_\odot$ yr^{-1})	Ω Ω	t_{end} (yr pre-SN)	dE/E_{sn} (per cent)	$v^a{}_{final}$ (km s^{-1}) 10^3 (km s^{-1})
O01	30	1	N/A	200	10^{-4}	0.0	N/A	0.05	4.39
O02	30	1	N/A	200	10^{-3}	0.0	N/A	0.3	3.42
O03	30	1	N/A	200	10^{-2}	0.0	N/A	1.5	2.57
O04	30	1	N/A	50	10^{-4}	0.0	N/A	0.108	3.75
A00	30	1	0.1	200	10^{-4}	0.0	2	0.8	2.85
A01	30	1	1	200	10^{-4}	0.0	2	5.05	2.34
A02	30	1	6	200	10^{-4}	0.0	2	18.7	1.79
A03	30	1	10	200	10^{-4}	0.0	2	25.5	1.59
A04	30	1	20	200	10^{-4}	0.0	2	36.5	1.27
A05	30	1	10	200	10^{-3}	0.0	2	25.6	1.51
A06	30	1	10	200	10^{-5}	0.0	2	25.3	1.61
A07	30	1	10	50	10^{-3}	0.0	2	31.5	1.30
A08	30	1	10	500	10^{-3}	0.0	2	16.9	1.66 (at 500 d)
A09	30	1	10	50	10^{-4}	0.0	2	31.6	1.36
A10	30	1	10	500	10^{-4}	0.0	2	16.3	1.80 (at 500 d)
A11	30	1	10	50	10^{-5}	0.0	2	31.6	1.46
A12	30	1	10	500	10^{-5}	0.0	2	16.3	1.80 (at 500 d)
B01	10	1	10	50	10^{-4}	0.0	2	54.5	1.52
B02	10	1	10	200	10^{-4}	0.0	2	48.2	1.83
B03	10	1	10	500	10^{-4}	0.0	2	37.0	2.12 (at 500 d)
B04	10	1	25	200	10^{-4}	0.0	2 ($\Delta t = 5$ yr)	65.1	1.08 (at 500 d)
C01	60	1	10	50	10^{-4}	0.0	2	19.7	1.18
C02	60	1	10	200	10^{-4}	0.0	2	14.5	1.30
C03	60	1	10	500	10^{-4}	0.0	2	7.55	1.46
D01	10	1	10	500	10^{-4}	0.9	2	42.1	N/A
D02	30	1	10	500	10^{-4}	0.9	2	20.4	N/A
D03	60	1	10	500	10^{-4}	0.9	2	10.9	N/A
E01	30	1	10	500	10^{-4}	0.0	4	14.7	1.79 (at 500 d)
E02	30	1	10	200	10^{-4}	0.0	10	24.3	1.62 (at 500 d)
E03	30	1	10	500	10^{-4}	0.0	10	13.9	1.79 (at 1000 d)
F01	30	0.5	10	200	10^{-4}	0.0	2	22.3	1.13
F02	30	2	10	200	10^{-4}	0.0	2	27.4	2.19
G01	6	1	6	200	10^{-5}	0.0	2	56.4	2.07 (at 100 d)
H01	1	1	1	200	10^{-5}	0.0	2	42.7	4.77 (at 100 d)

[a]Measured at 250 d unless indicated otherwise.

the SN expansion phase can be considered small. The inner radial boundary is fixed at $r = 0$ and does not move when the grid expands. The inner radial boundary and both azimuthal boundaries are set to reflecting boundary conditions so no matter can escape from the system.

3.2 Radiative cooling

In order to obtain a light curve from our simulation we include the effect of optically thin radiative cooling, using the cooling curve from MacDonald & Bailey (1981). We extend this cooling curve to temperatures above 10^{10} K by assuming that for these temperatures the cooling curve depends on the temperature as $\Lambda(T) \sim \sqrt{T}$ (i.e. bremsstrahlung).

Rather than use the cooling routine that comes as part of the ZEUS 3D code, we implement a new numerical method, described by Townsend (2009). This method uses exact integration of the radiative cooling function rather than the traditional implicit or explicit schemes. It is faster, more accurate and avoids the potential instability of the old radiative cooling method used in the ZEUS 3D code, which uses a Newton–Raphson implicit calculation scheme.

The assumption of *optically thin* radiative cooling to generate our light curves has some drawbacks. The circumstellar shells used in our simulations have high densities and are therefore likely to be optically thick to Thomson scattering if fully ionized. However, at such high densities, it is difficult for the material to remain fully ionized because of the fast recombination rates, we believe that our assumption is acceptable for our limited purposes, at least as far as radiation in the optical part of the spectrum is concerned. The high density of the circumstellar shells makes it unlikely that the ultraviolet light from the SN itself can fully ionize them. Those areas of the shell that become photoionized will undergo recombination on a very short time-scale. Typical mass density in the shell is about 5×10^{-13} g cm^{-3} (see Figs 1 through 8). Assuming pure ionized hydrogen for the sake of simplicity this gives us an electron density n_e of 6×10^{11} cm^{-3}. Dyson & Williams (1997) give a recombination rate of

$$\dot{N}_R = n_e^2 \beta_2(T_e) \tag{5}$$

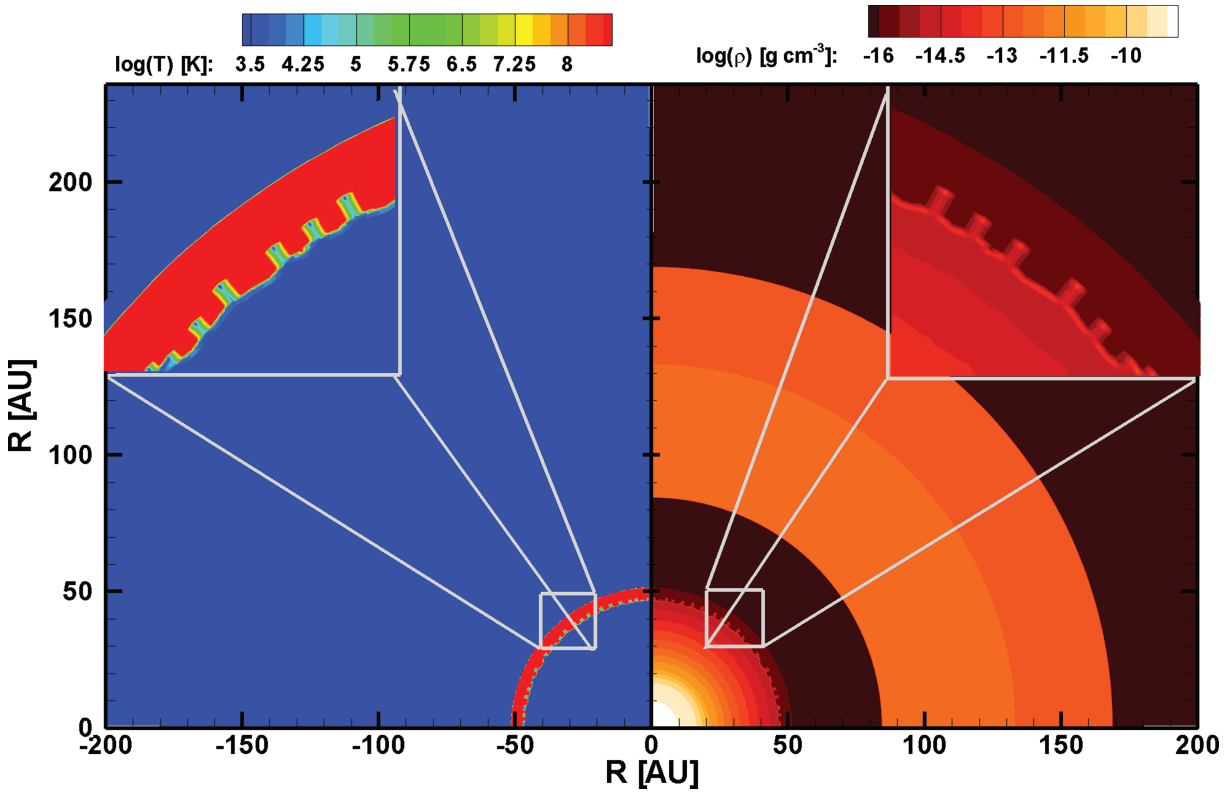

Figure 1. Temperature (left) and density (right) for simulation A03 at $t = 11.5$ d after the start of the simulation. The SN has not yet collided with the circumstellar shell. The front of the SN expansion (∼50 au) is clearly visible because of the high (∼10^8 K) local temperature. The small insets show how instabilities form in the thin SN shell. Clearly, we are at the limit of what can be achieved with this grid resolution.

with $\beta_2(T_e) = 2 \times 10^{-10} T_e^{-3/4}$ cm^3 s^{-1}. For an electron temperature T_e of 10 000 K, this gives us a recombination rate of 7.2×10^{10} per second. So even if fully ionized initially, the shell will recombine very quickly compared to the expansion of the shell. It takes the SN at least several days to reach the inner edge of the shell, so the effects of the initial ionization will most likely have disappeared by then, leaving only the remaining radiation from the expanding shock to photoionize the shell. This greatly reduces the number of free electrons that are available for scattering. Furthermore, although we use a shell with a smooth density structure (apart from the small random variations mentioned above), in reality circumstellar shells show a far more complicated structure of high-density filaments interspaced between low-density areas. Under these circumstances, the photons will tend to escape through the low-density regions (Owocki, Gayley & Shaviv 2004; Owocki & Cohen 2007). Finally, scattering by itself does not necessarily change the shape of the emerging light curve since a photon can escape with little modification even after multiple scatterings. Therefore, even though the electron scattering optical depth of our denser shells (under assumption of full ionization) can be as large as $\tau_e \geq 100$, the true optical depth will be much smaller due to efficient recombination.

The shape of the light curve will change if the diffusion time for photons to escape from the circumstellar shell gets close to the actual expansion time of the SN (Smith & McCray 2007). However, this is only likely to affect the light curves at early times; the net effect would be a slower rise time to peak luminosity and possibly a smoother peak, while diffusion is unlikely to substantially affect the overall efficiency of converting kinetic energy into radiation. The typical diffusion time-scale of a photon through the shell is $t_{diff} = \tau D/c$, with τ the optical depth, D the cross-section of the shell and c the speed of light, whereas the expansion velocity is $t_{exp} = D/V$. With the expansion velocity V typically below 2000 km s^{-1} (see the shell velocity plotted in Fig. 23 and also typical final velocities in Table 1) and lower for the denser, more optically thick shells, the photons have time to escape from the shell ahead of the expanding SN.

Although we have attempted to account for radiative cooling in a realistic way in our calculations, this is a difficult problem and our method is simplified and necessarily limited. Therefore, when interpreting our results, we concentrate on relative changes from one model to the next as we vary input parameters like mass and speed, rather than the absolute values of the luminosity for any individual model. As noted earlier, it is not our goal here to fit the observed light curve and derive corresponding physical parameters for any individual SN, but rather, we aim to understand how the variety of possible observed properties arises from different input parameters.

4 SN–CSM INTERACTION

Here, we describe the general properties of our SN–CSM interaction simulations. As an SN interacts with the CSM, we observe three phases dictated by our assumed input geometry: (1) a fast interaction between the SN and the (relatively) low-density wind inside the shell, (2) a slower interaction as the SN shock pushes into the much denser medium of the massive shell and (3) the final expansion phase as the SN has broken through the shell and continues to interact with the wind outside the dense shell.

To demonstrate the strong interaction between a core-collapse SN and a circumstellar shell, consider simulation A03 (Table 1),

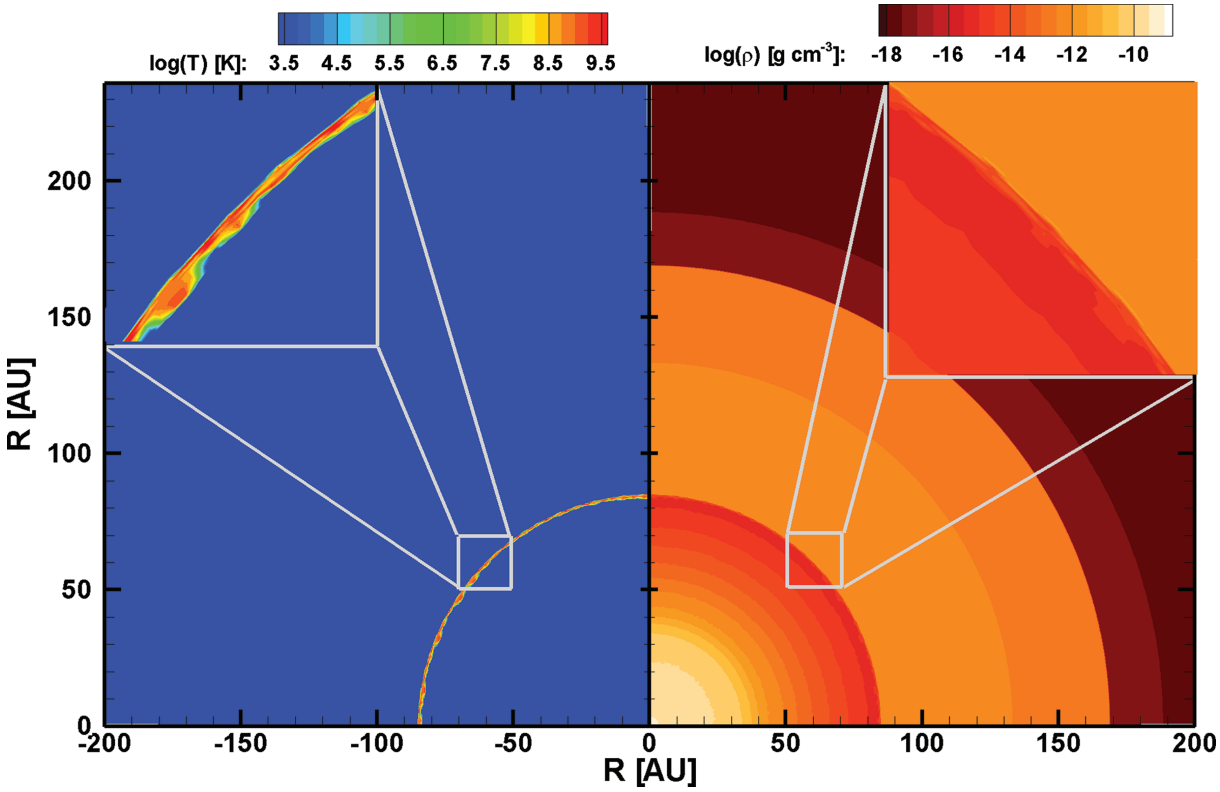

Figure 2. Similar to Fig. 1, but at $t = 23$ d. The SN ejecta have reached the circumstellar shell. Note that the high-temperature region has become extremely narrow. This is due to the high density of the shocked gas, which allows it to cool very rapidly. The temperature of the shocked gas increases, as more kinetic energy is converted to thermal energy. Again, the small figures show details of the SN shell, which is extremely thin. Local instabilities are small.

in which a $30\,M_\odot$ explosion collides with a $10\,M_\odot$ circumstellar shell moving at $200\,km\,s^{-1}$. Figs 1 to 4 show snapshots of the temperature and density of the expanding SN as it interacts with the CSM (movies of our simulations are provided in the electronic edition). The high post-shock density encountered because of the very massive CSM shells we use causes the radiative cooling to be extremely efficient in these simulations, sometimes reducing the internal energy of even the shocked gas to the point where the temperature reaches a minimum value of 1000 K.[1] (This lower limit is a matter of numerical convenience that we impose upon the calculation.) Since the temperature difference before and after cooling can be quite large, we show the temperature of the gas before the radiative cooling has been taken into account, which is more representative of the wavelength of the emitted radiation. This is the same temperature that we use to obtain the light curves in Section 5, adjusted for adiabatic expansion.

At first, the SN ejecta expand quickly as the forward shock encounters the stellar wind, creating a layer of hot (several times $\sim 10^8$ K), shocked gas (Fig. 1). At the inner boundary of this high-temperature zone (the reverse shock), SN material piles up and creates a shell. The interaction is (nearly) energy conserving at this point. When gas crosses the reverse shock, the kinetic energy of the SN is converted to internal energy and heats the shocked gas, pushing the forward shock into the CSM. The shell, which is very thin due to radiative cooling, is subject to thin-shell instabilities. However, these take time to form and the shell is expanding rapidly, which limits their opportunity to grow. As a result, the shell retains its basically spherical shape. Because only a small fraction of the SN material has a high velocity (see Section 2.1), the blast wave slows down quickly when it sweeps up the wind. This effect is greatly increased in the next phase when the SN ejecta collide with the dense circumstellar shell.

Initially, the collision between SN ejecta and a massive circumstellar shell causes a rapid decrease of the forward shock velocity. This deceleration drains energy from the forward shock, *and powers the main peak of the light curve*. The density at the forward shock increases sharply as the shock overtakes more of the massive circumstellar shell. The layer of hot, shocked gas is compressed as the reverse shock starts to overtake the forward shock, which leads to an increase in local temperature ($\sim 10^9$ K in Fig. 2). The high temperature, combined with the high density of the gas, makes the radiative cooling efficient. Therefore, the thermal pressure of the shocked gas does not increase further. This, combined with the compression between the two shocks, causes the hot gas layer to become quite thin and marks the transition from an energy conserving shock to a momentum conserving one.

As the forward motion slows, the shock temperature decreases. The cooling remains efficient, so the high-temperature region, which is now at about $\lesssim 10^5$ K, remains thin (see Fig. 3). The thin shocked gas layer is subject to radiative cooling instability (the higher density

[1] The fact that our calculations cool to a temperature as low as 1000 K with a standard cooling prescription has far-reaching implications for understanding dust formation in CSM-interaction SNe. This is not the topic of our study here, but recent observations of SN 2006jc (Smith, Foley & Filippenko 2008b) and 2005ip (Smith et al. 2009; Fox et al. 2009) have demonstrated that new dust grains are seen to condense in the post-shock gas at the same time when strong X-rays and high ionization emission lines are seen. With efficient cooling in the dense shock leading to the low temperatures in our simulations, dust formation may be a natural consequence.

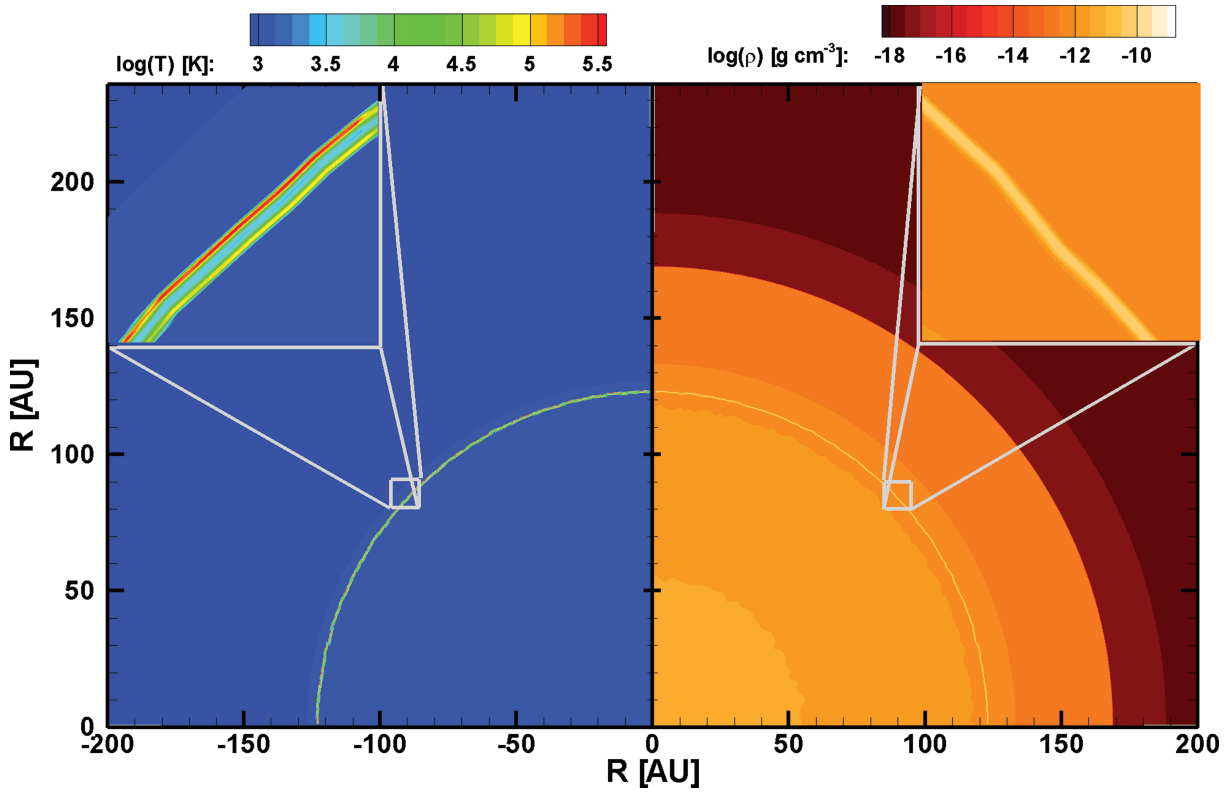

Figure 3. Similar to Figs 1 and 2, but at $t = 86.8$ d. The SN is approximately halfway through the circumstellar shell. The temperature of the shocked region is much reduced (to $\sim 10^5$ K), because the high density of the shell reduced the expansion velocity. The small figures show the thin high-temperature layers on each side of the shell. The shell is not perfectly spherical, but the instabilities are extremely small as they are compressed between the expanding SN and the high-density material of the shell.

regions cool more efficiently, leading to a loss of thermal pressure, which in turn leads them to be compressed to even higher density). This can be observed in Fig. 3 as variations in the local temperature in the shocked gas. However, like in the initial phase, the expansion of the SN occurs at higher velocity than the formation of the instabilities. Also, the shocked gas layer is compressed between two areas with very high density (the shell on the outside and the rest of the SN on the inside), which inhibits expansion apart from the bulk motion of the shock. Therefore, there is no significant departure from spherical symmetry.

Once the SN breaks through the shell, the forward shock may accelerate again due to the transition to much lower densities in the wind, though it will never reach the original high velocity because a large amount of energy has been lost to radiation during the shell collision phase. Also, the velocity of the unshocked SN ejecta piling up at the reverse shock decreases over time, limiting the shell's ability to accelerate in this later phase. As a result, the temperature of the hottest shocked gas is now limited to a few times 10^6 K (Fig. 4). The lower density at the interaction front makes the radiative cooling less efficient, which allows the hot gas layer to build up, though it never reaches its original size.

4.1 Bipolar nebulae

The collision between an SN and a bipolar nebula shows the same general pattern as described above, but is somewhat more complicated and modified by the shell geometry. Figs 5 through 8 show the same time frames for simulation D02, which models a collision between the same SN as in simulation A03 with a $10\,M_\odot$ shell, but here the shell is bipolar.

Initially (Fig. 5), the simulations look the same as before, but they diverge once the SN hits the circumstellar shell. This occurs first at the pinched equatorial waist of the nebula, where the shell radius is the smallest (Fig. 6). The collision squeezes the region of shocked gas into a very thin layer. In polar directions, the SN still expands into a lower-density wind and the hot gas layer remains wide. At a later stage, the interaction with the shell has slowed the expansion at the equator, leading to a lower shock temperature ($\sim 10^4$ K in Fig. 7), whereas the shock temperature at the pole is still high because the shock has only just reached the circumstellar shell and has not swept-up enough mass to decelerate yet.

Eventually, the SN will start to break out of the shell at the equator first, while it is still inside the shell at the pole (see Fig. 8). When this happens, the shock at the equator will reheat to about 10^6 K, while the temperature at the pole remains low. Since the circumstellar shell has most of its mass concentrated at the pole (where it also has the largest solid angle), it takes much longer for the SN to break out in that direction. As a result, the shock in the polar direction will always be less energetic afterwards than at the equator. Because of the different times when the shock hits the equatorial and polar regions of the shell, different shock temperatures can be seen simultaneously. We therefore suggest that simultaneous observations of multi-wavelength (i.e. X-ray and visual) light curves may provide a way to distinguish bipolar from spherical shells, as we describe in more detail later.

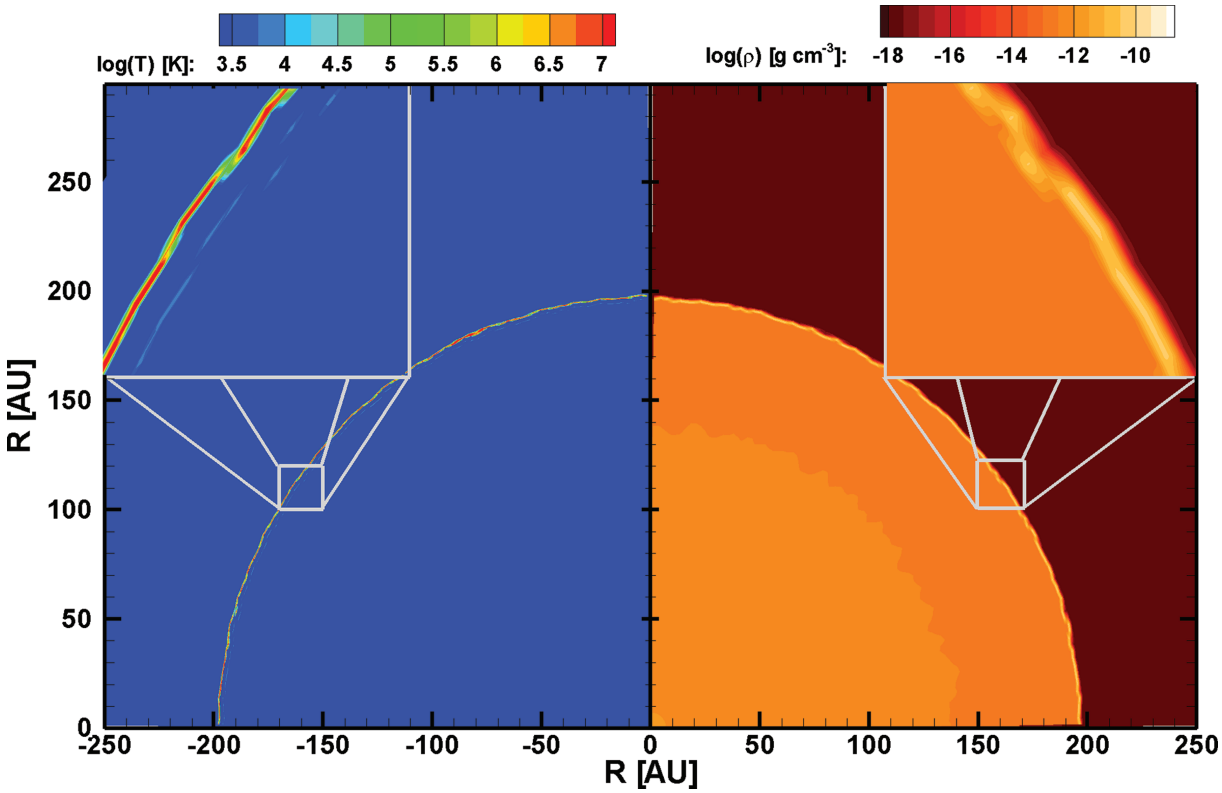

Figure 4. Similar to Figs 1 through 3, but at $t = 173.6$ d. The shock-heated layer remains extremely thin, indicating a nearly isothermal shock. The shock temperature has decreased because sweeping up the circumstellar matter slows down the SN expansion. The instabilities are somewhat larger now, but remain small compared to the overall scale of the expansion.

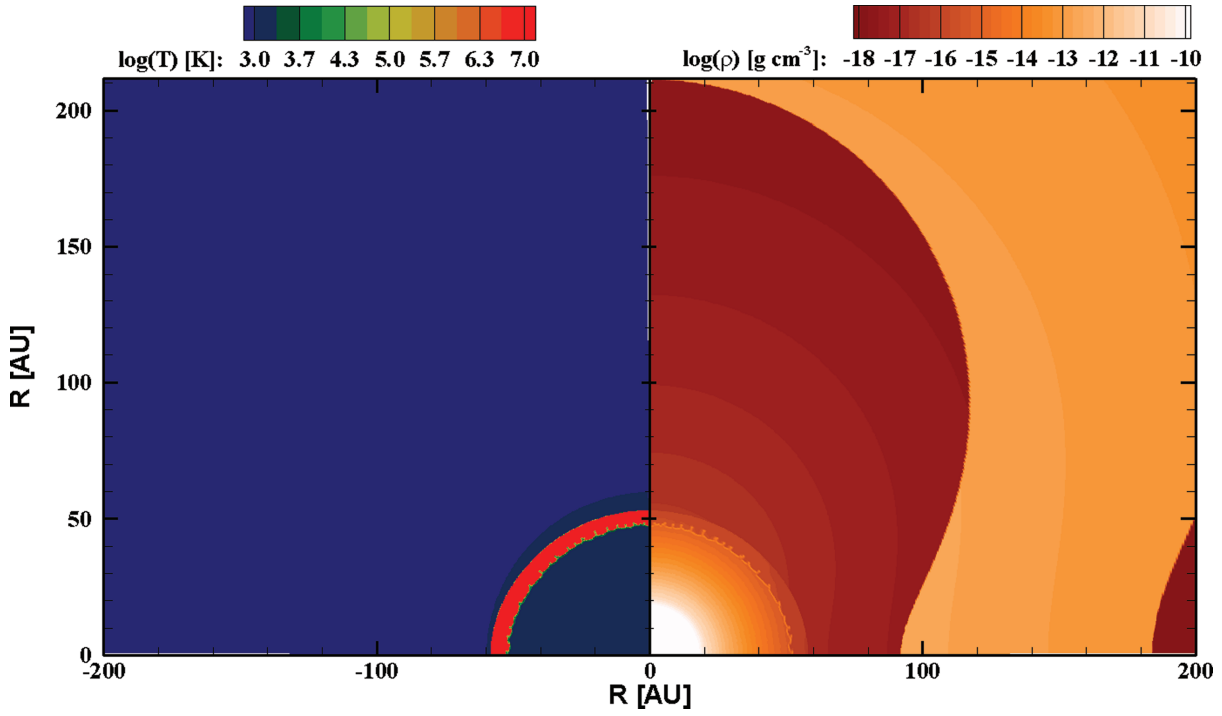

Figure 5. Temperature (left) and density (right) for simulation D02 at $t = 11.5$ d after the start of the simulation. This is the equivalent of Fig. 1, but with a bipolar nebula. At this point in time the SN expansion is almost identical to the expansion in a spherical CSM.

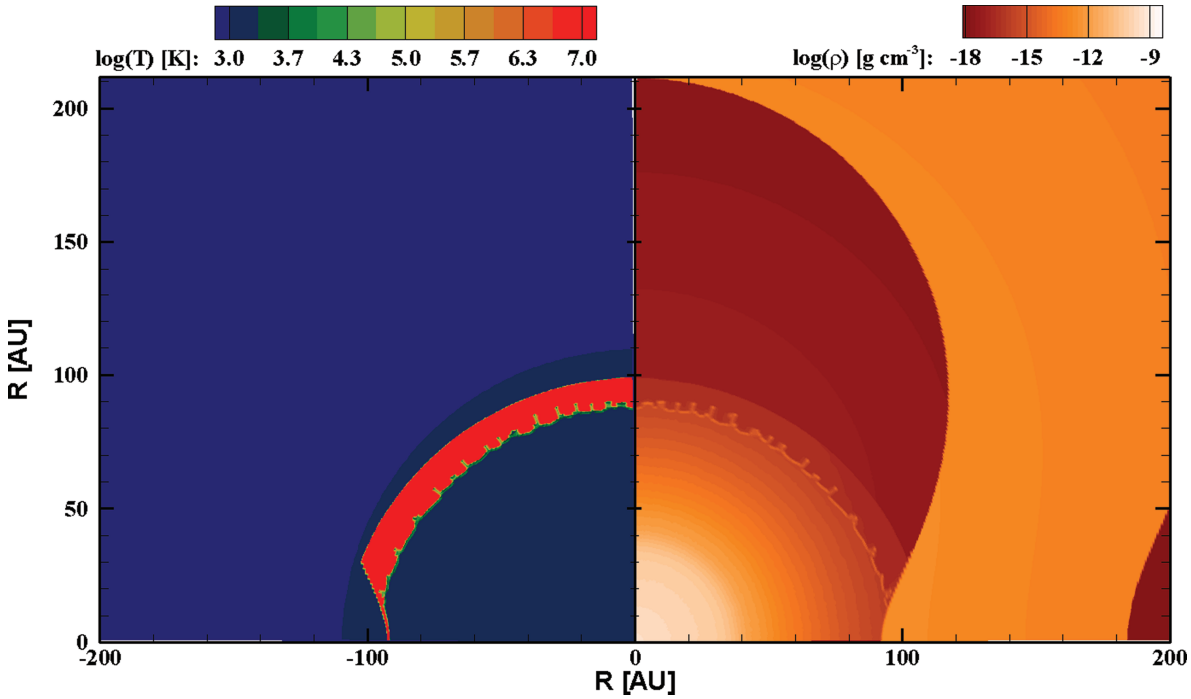

Figure 6. Similar to Fig. 2 (same time-step), but for simulation D02. At the equator, the SN has reached the shell and has been slowed down abruptly at the pole. The SN is still expanding into the wind. Note the difference in the hot gas layer, which has been squeezed by the collision.

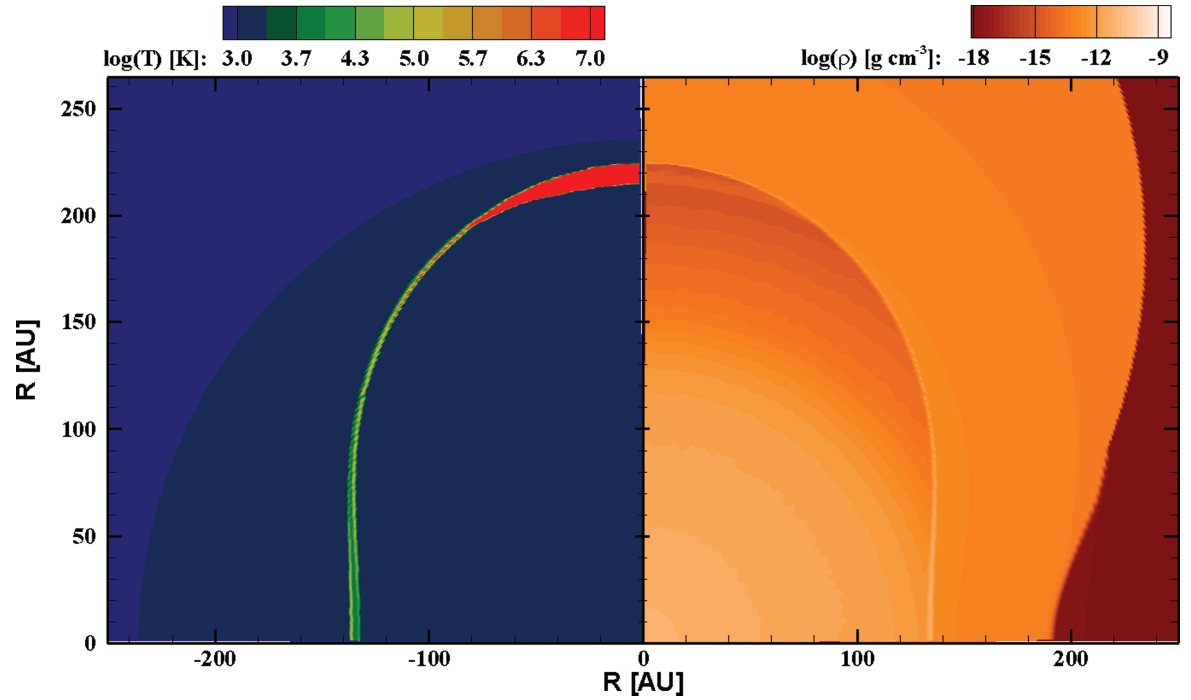

Figure 7. Similar to Fig. 3 (same time-step), but for simulation D02. At the equator the SN is moving through the shell. The slow shock has reduced the temperature of the hot gas zone to about 10^4 K. At the pole the SN has finally reached the circumstellar shell. There the hot gas is still at a high temperature (10^7 K).

5 SUPERNOVA LIGHT CURVES

5.1 General properties

The assumption of optically thin cooling, though a reasonable approximation in optical wavelengths, breaks down for high frequencies. Most likely, for massive shell collisions, the early-time X-rays and UV would be completely self-absorbed and reprocessed into visual-wavelength luminosity. Therefore, rather than attempt to plot the emission as a function of the gas temperature, we concentrate on the bolometric luminosity light curves as a likely proxy for the visual light curves in later sections; this assumption may break down

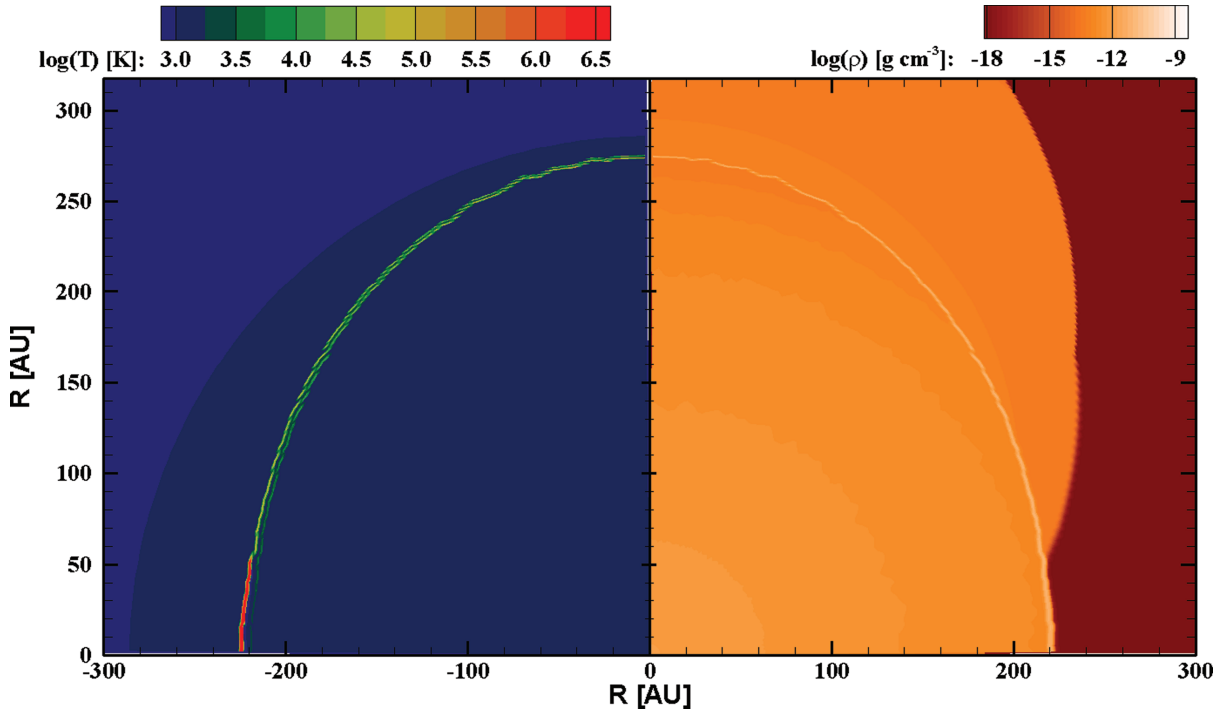

Figure 8. Similar to Fig. 4 (same time-step), but for simulation D02. The SN has broken through the shell at the equator, but is still plowing through it at the pole. The temperature at the equator is now high again ($\sim 10^6$ K), whereas the shock over the pole has slowed down, lowering the local shocked gas temperature.

at late times when the shock becomes optically thin and X-rays can escape (see below). In addition, it is important to note that our light curves correspond only to radiative energy losses from the post-shock gas. We do not include the photospheric emission from the underlying SN itself, which could, in principle, be any type of SN. (It is the shell collision that leads to a Type IIn spectrum and the enhanced luminosity, rather than any intrinsic property of the SN.)

As is shown below, the overall shape of the light curve for any SN–CSM collision model has the same general properties. Initially, the SN expands into the (relatively) low-density wind, starting at high luminosity due to its high velocity. As the expanding shock sweeps up more wind material, the expansion speed is reduced and the light curve shows a corresponding decrease in luminosity.

Note that the behaviour in this early phase – while the shock propagates through the wind on its way to reach the inner radius of the dense shell – depends strongly on our assumed value for the inner radius of the shell and on the assumed time before the SN when the shell ejection finished ($t_{\rm end}$ in Table 1). If the SN had occurred immediately after the shell ejection stopped or while it was still in progress, then this early phase would not exist. This may be an important consideration in determining the early light-curve shape: some luminous SNe like SN 2006gy and SN 2005gj show a long and slow rise to peak luminosity (Smith et al. 2007; Prieto et al. 2007), while others are discovered at peak and decline immediately, as in the cases of SNe 1998S, 1997cy and 2006tf (Leonard et al. 2002; Germany et al. 2000; Smith et al. 2008a), suggesting a very rapid initial rise time.

When the SN reaches the circumstellar shell, which takes on the order of 10–25 d in most of our simulations, the expansion decelerates abruptly. This shows up as a rapid increase of the emission, because the fraction of kinetic energy converted into thermal energy is now high. Also, the very high density of the shocked gas causes it to radiate very efficiently. As the SN plows through the shell, the emission decreases again due to the general decrease in shock velocity, but remains high compared to the emission from the initial phase.

Once the SN has overtaken the massive shell and begins to expand into the outer low-density wind (at $t \simeq 140$ d), the total emission decreases because the density of the gas that the SN collides with has decreased. Unlike the previous phases while the blast wave was expanding inside and through the massive shell, the densities are relatively low, and so optical depth effects are less likely to cause complete self-absorption of high-energy photons. Thus, once the blast wave has broken through the outer boundary of a hypothetical massive shell, we would predict that soft X-ray emission could in fact be observed. Mass-loss rates derived from observations of this X-ray emission would trace the normal wind mass-loss rate of the progenitor star in the years *before* it ejected the massive dense shell that led to the enhanced optical luminosity; meanwhile, the optical luminosity is still being emitted by the dense shell. Therefore, one would not necessarily expect agreement in mass-loss rates derived from observed optical and X-ray luminosities (see e.g. Smith et al. 2007). As the SN blast wave continues to expand into the wind, it gradually decelerates because the amount of swept-up gas increases over time. This leads to a steady and slow reduction in total emission in the years after the initial collision.

Since both the circumstellar shell and the SN are spherically symmetric, the collision happens at the same moment everywhere. Similarly, the SN will break through the shell at the same time all around its circumference. As a result, both sides of the main peak in the light curve have very steep slopes, and the change in X-ray emission would most likely be quite sudden. This is partly a result of our prescribed geometry of the shell, with a clean inner and outer boundary. Real circumstellar shells can show a wide variety of different geometries, including multiple shells and high degrees of clumping, which can vastly change the appearance of the light

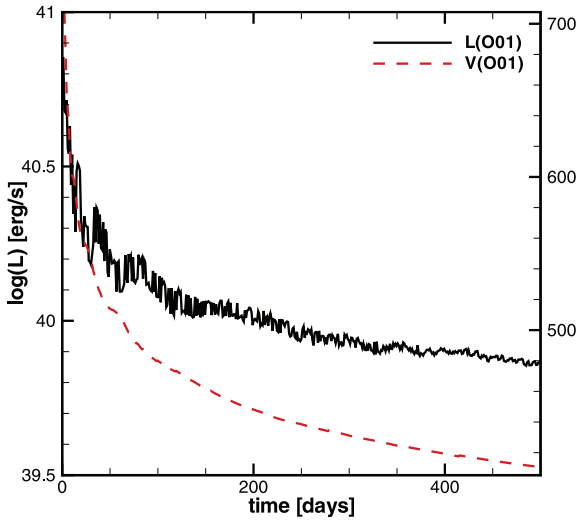

Figure 9. Light curve and reverse shock velocity for an SN expanding into a CSM that contains only wind (simulation O01).

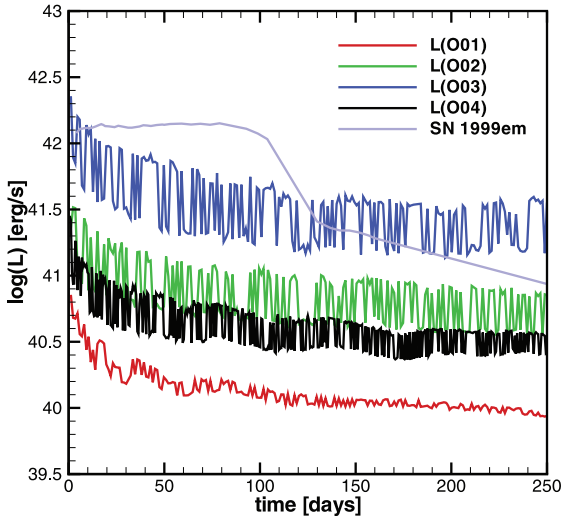

Figure 10. Light curves for four simulations without circumstellar shells. (O01–O04) In most cases the luminosity falls well below peak values for a typical SN II-P photosphere ($\sim 10^{42}$ erg), illustrated by the observed light curve of SN 1999em (Leonard et al. 2002).

curves. As one example, we explore the influence that a bipolar shape has on the emergent light curve. Our point here is not to provide an exhaustive grid of simulations of possible light curves, but to simply illustrate the behaviour as we vary the parameters of the collision in order to guide the interpretation of light curves of luminous SNe. The responses of the light curves to various parameters of the wind and shell are described in the following sections.

The most important consequence of the SN–shell collision is that SN kinetic energy is converted to thermal energy and then lost to radiation. The efficiency of this conversion is a key parameter for interpreting the energy budgets of SNe IIn. For each simulation discussed below, we list the total efficiency in converting kinetic energy into radiated energy over the course of the simulation, $E_{\rm rad}/E_{\rm SN}$, in the second to final column of Table 1. We find a large range in the conversion efficiency, depending on the mass of the shell as well as the mass of the SN. For a circumstellar shell mass of 10 $M_\odot$, the efficiency is typically 15–30 per cent. Efficiency increases with increasing density of the circumstellar shell (higher shell mass, slower velocity or both). The efficiency also increases for lighter SNe (higher ratios of $M_{\rm shell}/M_{\rm SN}$), because of momentum conservation and the greater deceleration of the fast SN ejecta. We elaborate on these points for individual cases below.

5.2 No shell, Just a wind

Since we are interested in investigating the effects of various properties of massive circumstellar shells, one might first ask what the collision looks like when there is no shell – i.e. when it is simply a collision between the SN and a dense steady wind. Fig. 9 shows the bolometric luminosity emission light curve and the shock velocity (See Section 6) for a simulation where the CSM contains no shell (O01), but just a dense wind with $\dot{M} = 10^{-4}$ $M_\odot$ yr^{-1} expanding at a speed of 200 km s^{-1} as one might expect for a massive LBV progenitor (Smith et al. 2007, 2010; Trundle et al. 2008). Both the luminosity and post-shock shell velocity start high, but decline quickly as the SN sweeps into the dense wind.

However, an important point to take away from simulation O01 is that the peak luminosity at early times is less than 10^{41} erg s^{-1}, and is therefore likely to be dwarfed by much stronger emission from an underlying SN photosphere (not shown in Fig. 9). A normal Type II-P SN, such as SN 1999em (Fig. 10; Leonard et al. 2002), has a luminosity during a $\sim$110 d plateau of $\sim 10^{42}$erg s^{-1}. This is 100 times stronger than the day 100 luminosity in simulation O01. Even SN 2005ip, which represents the lower end of luminosities for Type IIn core-collapse SNe, had a late-time luminosity due to circumstellar interaction of $10^{41.5}$ erg s^{-1} (Smith et al. 2009; Fox et al. 2009). The main consequence is that the more luminous class of SNe IIn require massive circumstellar shells, ejected in outbursts occurring shortly before core collapse – rather than steady winds – as emphasized elsewhere (Smith et al. 2007, 2008a; Smith & McCray 2007). This is also illustrated by a comparison between simulations O01 and A00. These have the same input parameters except for a very low mass (0.1 $M_\odot$) circumstellar shell in the case of A00. Despite the low mass, the shell causes the total amount of energy converted to radiation to jump by more than an order of magnitude.

Winds with higher density, through either high mass-loss rates (O02 and O03) or low velocity (O04) tend to produce higher luminosities through the collision, as expected, but these enhancements are small compared to the effect of massive shells. (See also Table 1 for the percentage of energy converted into radiation.) The only 'no-shell' simulation to produce a higher luminosity than that caused by even the smallest circumstellar shell is simulation O03, which assumes a mass-loss rate of 10^{-2} $M_\odot$ yr^{-1}. Interestingly, this high wind mass-loss rate produces a late-time plateau with a luminosity of $\sim 10^{41.5}$ erg s^{-1}, appropriate for the late phases of SN 2005ip (Smith et al. 2009; Fox et al. 2009). A similar progenitor mass-loss rate was inferred for SN 2005gl, which had an LBV-like progenitor identified in pre-explosion data (Gal-Yam & Leonard 2009). The shapes of these light curves also resemble SN 1988Z (Aretxaga et al. 1999), where the luminosity remained high for about a decade, indicating that the expanding SN interacted with an extended circumstellar wind, rather than a sharply confined shell. Such a mass-loss rate is in excess of even the strongest LBV winds in their quiescent states (i.e. 10^{-3} $M_\odot$ yr^{-1} in the case of η Car; Hillier et al. 2001), but is comparable to smaller LBV eruptions like the 1600 AD event of P Cygni (Smith & Hartigan 2006) or the 1890 eruption of η Car (Smith 2005). In other words, a steady 'wind' with

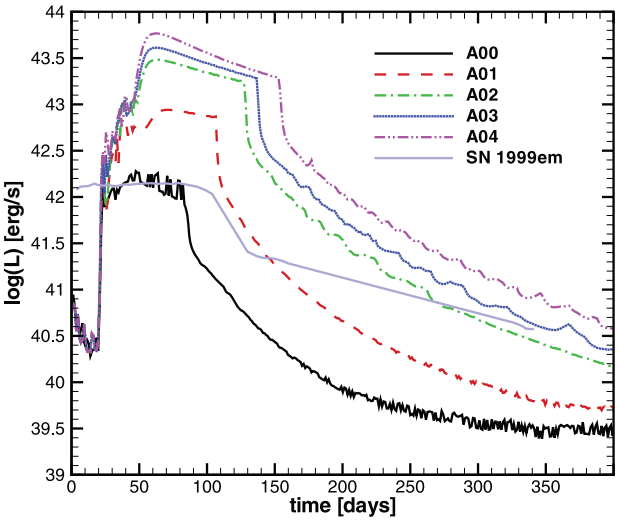

Figure 11. Total bolometric luminosities for simulations A00 through A04 as a function of time. The higher shell masses cause higher luminosity peaks, for all other explosion and shell parameters held the same. Higher shell masses also cause more deceleration, so the shock takes longer to break through the shell, leading to a longer lasting peak in the light curve. Both the beginning and the end of the luminosity peak are marked by a sharp transition in all simulations, which results from our assumed inner and outer boundaries of the shell. The light curve of the SN II-P 1999em is shown again for comparison, as in Fig. 10.

$\dot{M} = 10^{-2}\,\mathrm{M}_\odot\,\mathrm{yr}^{-1}$ is essentially the same as a sustained eruption (i.e. the total mass swept up by the shock is comparable). This is also the only simulation without a shell for which the radiative luminosity exceeds values typically expected from the SN photosphere (Fig. 10). One can expect that steady winds or sustained eruptive phases with even higher mass-loss rates or slower wind speeds will result in long-lasting light curves shaped like those in Fig. 10, but with even higher luminosity.

5.3 Shell masses

The next group of simulations in Table 1 (A00 to A04) explore the effect that the circumstellar shell mass has on the evolution of the SN light curve. Fig. 11 shows the total bolometric radiative luminosity for each simulation as a function time, compared to the light curve of a normal SN II-P. Because it takes more energy to break through a more massive shell, more kinetic energy is converted to thermal energy and then to radiative energy loss. Therefore, the higher the shell mass, the higher the luminosity peak. Also, it takes longer to break through a high mass shell, because the shock suffers more deceleration, so the duration of the peak luminosity will be longer for higher mass shells as well. It is noteworthy that even the lowest mass shell ($0.1\,\mathrm{M}_\odot$) simulation, A00, shows a clear peak and is therefore distinguishable from the pure wind interactions shown in Fig. 10, although in practice this peak might be lost amid the photospheric emission from the SN itself.

All shells show sharp transitions at the beginning and the end of the main luminosity peak, but this is a direct result of our prescribed sharp inner and outer boundaries of the shells. It is a simplifying assumption and is motivated by the observed sharp outer boundary in some dense shells around massive stars, such as the Homunculus of η Carinae (Smith 2006), but it is not necessarily true in all cases. It is likely that some objects will have smoother density transitions at the outer extent of the shell, and in those cases one expects the CSM-interaction luminosity to drop more gradually. The plateau is almost horizontal for the lower mass shells in our study, but changes to a shallow decrease with time for high-mass shells. This decrease results from the fact that the high-mass shells decelerate the blast wave to a greater extent as it plows through the shell. The decrease in shock speed leads to a reduction in post-shock thermal energy and a lower emergent luminosity.

5.4 Wind parameters

In our simulations, we vary both the wind velocity and mass-loss rate to explore the influence of these parameters on the light curve. Fig. 12 shows the effect of the wind mass-loss rate and velocity on the bolometric SN light curve, by comparing simulations A07, A09 and A11 (left-hand panel in Fig. 12), which have identical parameters except for the wind mass-loss rate, which is $10^{-3}, 10^{-4}$ and $10^{-5}\,\mathrm{M}_\odot\,\mathrm{yr}^{-1}$, respectively. In these simulation, the wind (and shell) velocity is fixed at $50\,\mathrm{km\,s}^{-1}$. In the initial stage, the difference is considerable, as the higher density winds clearly create much stronger emission. Also, the high wind density in simulation A05 actually slows down the SN expansion more than the other two, delaying the moment when the expansion reaches the shell, though not by a large amount. Since the shells are identical, the light curves all have the same peak in the light curve. After the circumstellar shell has been swept up, the difference between the light curves is difficult to see. The $10\,\mathrm{M}_\odot$ shell slows down the SN expansion to such an extent that the effect of the wind mass-loss rate becomes negligible. Still, after more time passes the curves start to diverge, albeit slowly, with once again the highest mass-loss rate creating the highest emission.

The middle and right-hand panels of Fig. 12 show the same phenomena, but for wind (and shell) velocities of 200 and $500\,\mathrm{km\,s}^{-1}$, respectively. The results follow the same pattern. However, due to the higher velocities, the densities are generally lower. As a result, the influence of the wind mass-loss rates in the final stages is lower for the simulations with wind velocity of $500\,\mathrm{km\,s}^{-1}$.

Comparing the three panels of Fig. 12 shows the effect of wind velocity on the light curve. Obviously, lower wind velocities mean that the shell is closer to the star when the SN hits it, which means that the entire time-frame of the interaction gets shortened. Also, the density in the shell is higher ($\rho \sim 1/v$), whereas the cross-section of the shell is smaller, leading to a higher, narrower peak in the luminosity.

5.5 Supernova masses

Letting three different SNe interact with the same circumstellar shell produces the light curves shown in Fig. 13, which shows the bolometric light curves for three different SN masses (10, 30 and $60\,\mathrm{M}_\odot$: colour-coded lines), colliding with three different circumstellar shells (velocities at 50, 200 and $500\,\mathrm{km\,s}^{-1}$: left, centre and right, respectively). All three circumstellar shells have the same mass of $10\,\mathrm{M}_\odot$.

These light curves show two characteristic patterns: because the kinetic energy in the SN is the same for all three simulations, the lower mass SNe have higher initial velocities. As a result, the peak in luminosity that results from the collision between the SN expansion and the circumstellar shells occurs earlier, and the peak luminosity is higher because of the greater energy per unit mass that is lost to radiation when the material is decelerated. The low-mass SNe have less momentum ($m_{A09}v_{A09}^2 = m_{B01}v_{B01}^2$ and $m_{A09} = 3m_{B01}$ so $m_{B01}v_{B01} = m_{A09}v_{A09}/\sqrt{3}$), so they slow down and give up their

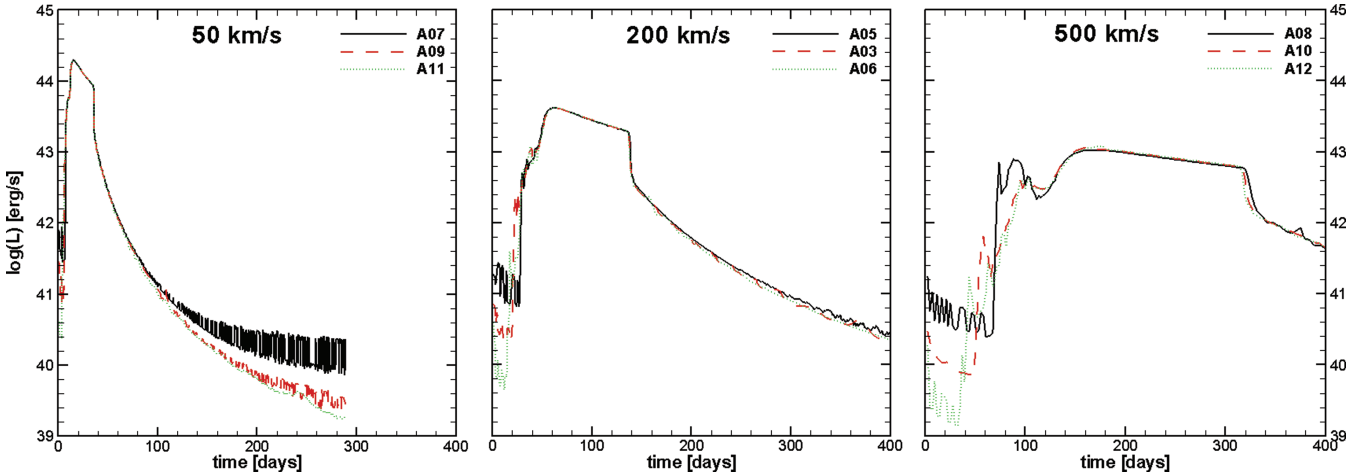

Figure 12. Total radiative emission light curves for circumstellar matter with different velocities (50 km s^{-1} in the left panel, 200 km s^{-1} in the middle and 500 km s^{-1} on the right) and different wind mass-loss rates (colour-coded lines). Obviously, the wind velocity has a major influence, since it determines how far the shell has travelled before the SN hits it. Wind mass-loss rate makes very little difference, except in the very early stages.

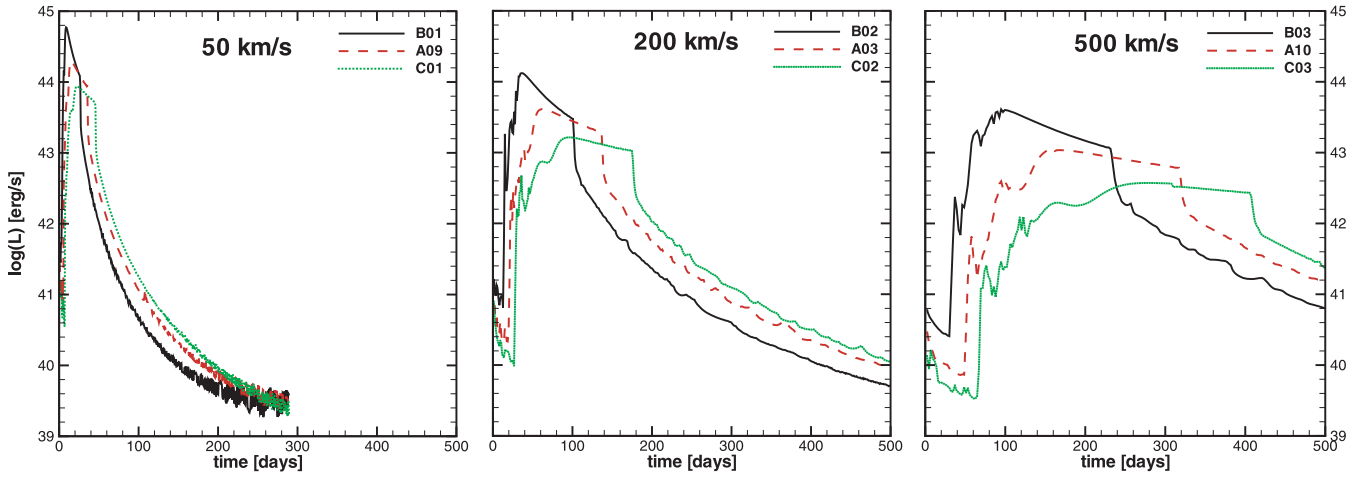

Figure 13. Total radiative emission light curves for collisions with different SN mass and wind velocities. The higher the SN mass, the lower the emission, as the high-mass SN has a relatively low velocity.

kinetic energy more quickly during the collision. As a result, the 10 M$_\odot$ SN produces a light curve where the flat plateau in the light curve peak is sharply angled, rather than horizontal as for the higher mass SNe. The slope of this plateau may therefore provide a useful diagnostic to constrain the mass and momentum ratios of the underlying SN and CSM shell. This same pattern can be seen in all three figures. The essential result is that relatively lower-mass SNe (i.e. faster SNe) have higher efficiency in converting kinetic energy into radiation, while more massive SNe have more momentum and therefore lose less of their kinetic energy to radiation. This is exactly the opposite of the effect of the shell mass, which produces a higher efficiency when the shell is more massive. Therefore, the highest efficiency will be achieved for those collisions wherein a relatively low-mass SN collides with a relatively high-mass shell (see also Fig. 24).

The influence of the wind and shell velocity is similar to that observed in Fig. 12. Higher expansion speeds stretch out the duration of the light curve and lower the peak luminosity, because the collision takes place later and over a longer time, and the shock plows through a lower-density shell for the same shell mass.

Extreme cases of low SN mass can be seen in Fig. 14, which shows the light curves for simulations G01 and H01, where SNe of 6 M$_\odot$ and 1 M$_\odot$, respectively, collide with shells of equal mass. The resulting light curves show peaks with extremely high luminosity ($\sim 10^{45}$erg s^{-1}), comparable to those of the most luminous SNe observed to date (Ofek et al. 2007; Quimby et al. 2007; Miller et al. 2009; Gezari et al. 2009; Smith et al. 2010). However, due to the low masses of the circumstellar shells, the bright peak fades quickly as the shell is swept up within just a few weeks, which is faster than the observed examples.

5.6 Supernova energy

Altering the total energy of the initial SN explosion can also change the apparent shape and luminosity observed in the light curve during its collision with a circumstellar shell. Indeed, in the case of SN 2006gy, Smith et al. (2010) measure a total energy ($E_{\rm rad}+_{\rm kinetic}$) of at least 5 $\times$ 10^{51} erg. Fig. 15 shows the light curves resulting from simulations F01, A03 and F02, where three different SNe of the same mass but kinetic energy of 0.5, 1 and 2 $\times$ 10^{51} erg,

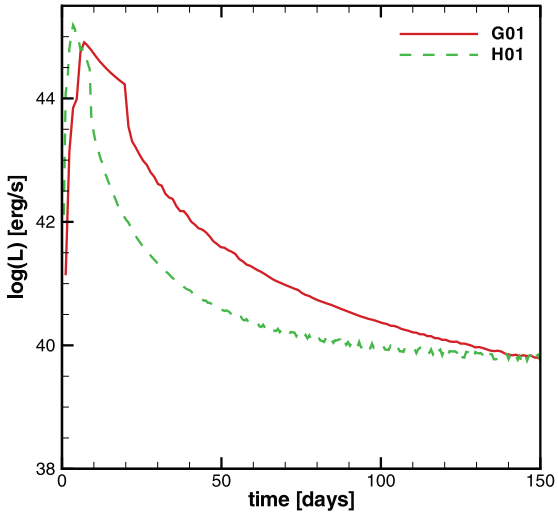

Figure 14. Light curves for two low-mass SNe (G01 and H01) with low-mass shells. The collisions are extremely luminous, but fade quickly.

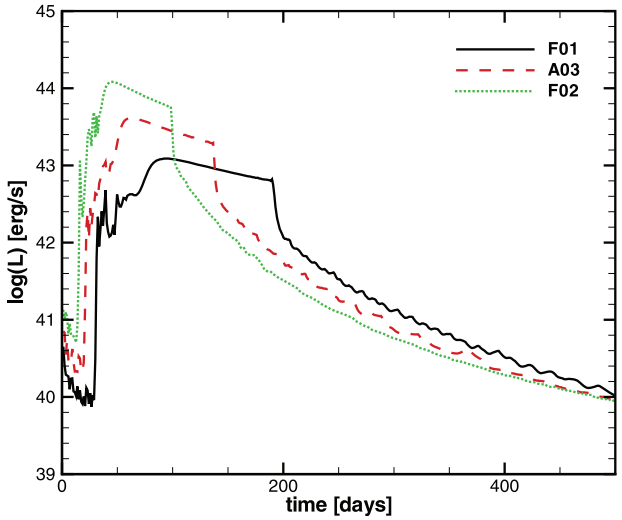

Figure 15. The influence of SN kinetic energy on the light curve. The higher the total energy, the higher the peak in the light curve and the shorter its duration, due to the increase in velocity.

respectively, all collide with the identical circumstellar shell of 10 $M_\odot$ expanding at the same speed of 200 km s^{-1}.

In the above discussion, we found that higher SN ejecta speeds and lower SN masses (a result of assuming that they all have the same explosion energy of 10^{51} erg) were key factors contributing to a high peak luminosity. The key ingredient of higher ejecta speeds can also be achieved with more total energy in an explosion, so we explored this as well. As one might naturally expect, more energetic SNe lead to higher peak luminosities because they give up more of their initial energy as their faster ejecta suffer a sharper deceleration during the collision. The light curve peak is also narrower (shorter in duration) for the more energetic and faster SNe because it takes less time to overrun the same shell.

The net effect of altering the SN energy is similar to that of changing the SN mass (but keeping the same energy), mainly because of the strong influence of the SN ejecta speed (i.e. compare Fig. 14 to the middle panel of Fig. 13). Comparing F01, A03 and F02 in Fig. 15 and Table 1, we see that SNe with higher explosion energy had higher peak luminosities, but also more total radiated energy

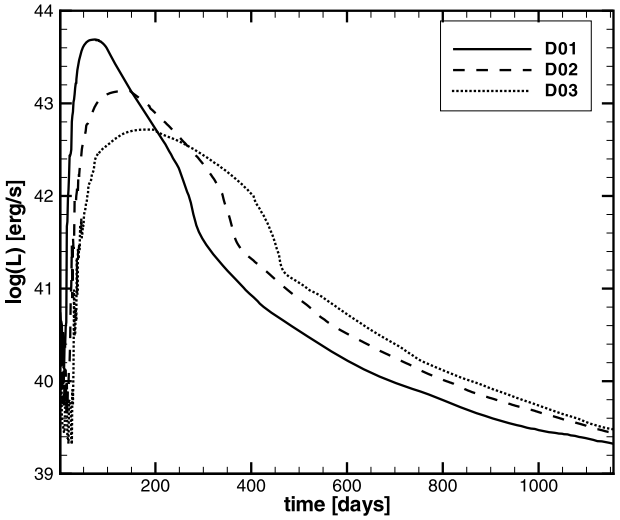

Figure 16. Bolometric light curves for the collision between three different SNe with $m = 10$ (B01), 30 (A09) and 60 (C01) $M_\odot$ and a bipolar circumstellar shell. The Peaks in the light curve show the highest luminosity for the lowest mass SN just as in Fig. 13. The peaks are much rounder than for the collisions between SNe and spherical shells.

and higher efficiency in converting shock energy into radiation, due to their higher speeds as discussed above. As we will see below, a major difference between these three SNe of different initial kinetic energy is seen in their final blast-wave speed after the shock overruns and exits the circumstellar shell, providing a potentially useful observational diagnostic (see Section 6).

5.7 Bipolar nebulae

So far, all our light curves have resulted from the collision between a spherical SN and a spherical circumstellar nebula. In contrast, Fig. 16 shows the bolometric light curve produced by the collision between the three SNe of three different masses and a 10 $M_\odot$ bipolar nebula. Fig. 16 is analogous to Fig. 13, but with a range of speeds in a single shell as a result of its bipolar geometry instead of a range of speeds in three different spherical shells. As with the spherical nebulae, the lower mass SNe tend to produce higher peak luminosity in the bipolar case because of their higher SN ejecta speeds. However, unlike the collisions between SNe and spherical nebulae, the luminosity peaks have smooth curves and more gradual slopes, somewhat reminiscent of the light curve of SN 2006gy (Smith et al. 2007). In our simulations, at least, this smoothness results from the bipolar shape of the nebulae. Rather than an instantaneous collision between the SNe and a circumstellar shell, the interaction starts gradually, with the collision beginning first at the equator and then eventually spreading to the pole. An analogous transition happens when the SN breaks out of the shell. Again, this happens first at the equator and only much later in the polar region. As a result, shocked gas regions with radically different temperatures and densities can exist simultaneously, as shown in Figs 5 through 8. One might imagine that a smoother light curve may also result from a smoother transition in density at the outer boundary of the shell.

A side effect of this situation would be that the possible onset of X-ray emission would be more gradual and not coincide with the drop in total luminosity as the SN breaks out of the shell. The X-ray curves are expected to be strong when the SN collides with a wind rather than a shell, both due to higher shock velocity

and lower optical depth. If the shell is spherical this transition happens everywhere at the same time. In the case of the bipolar shell, the SN breaks out at the equator long before it can break out at the pole. Therefore, part of the shock may already generate observable high energy photons, while another part is still plowing slowly through the shell and emitting at much lower temperature with all high energy emission being absorbed. Again, this effect may be relevant to the well-studied case of SN 2006gy, where the progenitor mass-loss rate inferred from the observed X-ray emission and Hα luminosity is in severe disagreement with the mass-loss rate needed to power the continuum luminosity in a CSM interaction scenario (Smith et al. 2010). From Figs 5 through 8, one might understand this apparent contradiction if, for example, the X-rays are generated at the equator where the forward shock has already broken through the shell, whereas in the polar region the shock is still plowing through the dense massive shell and thereby powering the continuum luminosity.

5.8 Time frames

If the time interval between shell ejection and the SN changes, this too will influence the shape of the light curve. We investigate this effect with simulations E01, E02 and E03, with the resulting light curve shown in Fig. 17. If there is a longer interval of time between the precursor shell ejection and core collapse, there are two effects. First, a given shell can travel further away from the star and will therefore have a lower density for the same shell mass. This will reduce the peak luminosity resulting from the shock interaction. The second effect of a larger time lag between shell ejection and core collapse is that it delays the onset of the strong CSM interaction phase. This can potentially lead to a second light-curve peak if one also considers the initial rise and fall of photospheric emission of the underlying SN that we do not include here.

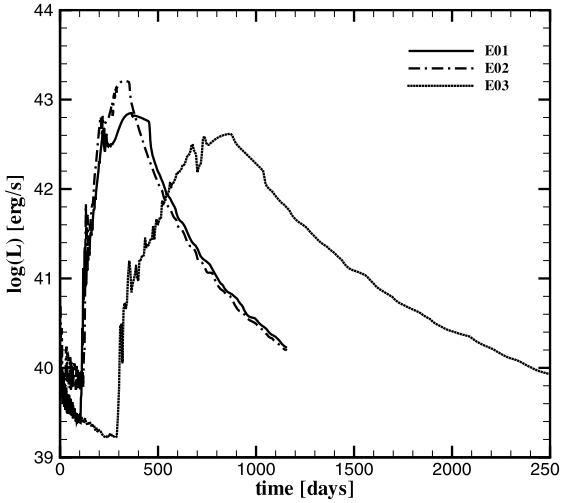

Figure 17. Bolometric light curves for the collision of a 30 $M_\odot$ SN and three 10 $M_\odot$ shells, ejected at different times and velocities. The parameters of simulations E01 and E02 have been chosen in such a way that the inner boundary of the shell is at the same position, though moving with different velocities. As a result, the light curves are nearly identical. Simulation A03 shows the light curve that results from collision with a shell that is much farther away from the star. As a result the peak in the luminosity is much shallower.

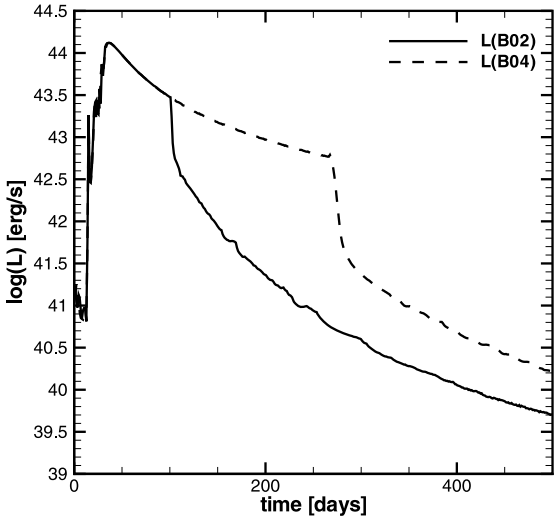

Figure 18. Total luminosity for simulations B02 and B04, demonstrating the effect of having a shell ejection that lasted over a longer period of time, making a thicker shell. These simulations are identical at first, except that the CSM shell in B04 has a larger outer radius at the same density, and thus has a higher total shell mass and remains at high luminosity for a longer time as the blast wave plows through this additional material. Since the cross-section of the shell is larger for B04 the peak in luminosity lasts much longer.

For simulations E01 and E02, the shell velocities and ejection times have been chosen so that the inner boundary of the circumstellar shell is at the same position for both shells, though they are moving at different speeds. As a result, the light curves are quite similar in onset and duration despite their different speeds. Due to the difference in shell velocity, the shell in E02 is denser than in E01, resulting in a higher luminosity peak, which, however, quickly disappears as the shock slows down. Generally, the lower density of these shells ($\rho \sim 1/r^2$) results in lower luminosity peaks more than 1 yr after core collapse, with edges that are less steep. They do not show the round peaks observed for bipolar shells (16). This effect is seen most clearly in light curve of simulation E03, which is extremely slow in its evolution, remaining luminous for several years.

Another parameter is the outer boundary of the massive shell, determined in our simulations by the duration of the shell ejection episode and the speed of the shell. In all simulations discussed so far, the duration of the shell ejection phase was $\Delta t = 2$ yr, and we varied the outer radius of the shell by adjusting the speed of the shell. However, the *duration* of the shell ejection can vary as well. The 19th century eruption of η Carinae, for example, lasted about 20 yr (Davidson & Humphreys 1997), although the mass ejection seems to have been concentrated in a shorter time interval (Smith 2006). If the shell ejection occurs at the same mass-loss rate but lasts longer, then the shell will be thicker and have a larger total mass. The main effect of this is that the main peak of the light curve would last longer at a comparable luminosity. This is indeed the case, as we show in Fig. 18, which compares simulations B02 and B04. This is different from the case mentioned above referring to the speed of the shell. If a larger outer radius and longer duration to the light curve result from a faster shell speed, then the density is lower for the same mass and the resulting luminosity will be much lower (compare simulations B01, B02 and B03).

6 SUPERNOVA SHELL VELOCITY

An important observational parameter for SNe IIn, in addition to their radiative luminosity and total radiated energy measured from light curves, is the expansion speeds measured from linewidths in spectra. In most SNe, the ejecta expansion speeds are inferred from P Cygni absorption features in the photospheric spectra, and this can be done in SNe IIn if the underlying photosphere can be seen (Turatto et al. 1993; Chugai & Danziger 1994; Salamanca, Terlevich & Tenorio-Tagle 2002; Smith et al. 2009). Often, however, the underlying SN photosphere is masked by the bright and possibly opaque emission from the dense shell of post-shock gas that powers the excess luminosity in SNe IIn (e.g. Chugai et al. 2004; Smith et al. 2008a). Fortunately, the dense shell of shocked gas that piles up at the contact discontinuity in the SN–CSM collision can be seen in the intermediate-width wings of the narrow Hα emission lines, for example, and typically has a speed of a few 10^3 km s^{-1} (Turatto et al. 1993; Chugai & Danziger 1994; Fransson et al. 2002; Chugai et al. 2004; Prieto et al. 2007; Smith et al. 2007, 2008a,b, 2009, 2010).

In order to estimate how the presence of a circumstellar shell influences the velocity of the post-shock gas seen in Hα emission, we plot the velocity of shocked gas as a function of time: specifically, we plot the mass-averaged radial velocity of the gas between the forward shock ($R2$) and the reverse shock ($R1$)

$$v_{\rm av} = \frac{\int_{R1}^{R2}\int_0^{\pi} r^2 \sin(\theta)\rho v_r {\rm d}r{\rm d}\theta}{\int_{R1}^{R2}\int_0^{\pi} r^2 \sin(\theta)\rho {\rm d}r{\rm d}\theta}. \quad (6)$$

We choose this method to quantify the shocked gas velocity because it gives a good result both in the adiabatic and in radiative shock regime. Mass averaging rather than volume averaging is more realistic since the luminosity is highly density dependent, so high-density areas would dominate the emission.

The behaviour of the shocked gas velocity during the SN–shell collision generally proceeds as follows. Initially, the velocity drops exponentially, because the blast wave decelerates while sweeping up the surrounding wind. When the forward shock hits the circumstellar shell it practically halts and the reverse shock velocity drops abruptly as the gas between the two shocks is compressed. After the initial collision the shocked gas velocity increases again as the forward shock recovers. However, the velocity is now much lower since the interaction has become radiative, so much of the available energy has already been lost. Also, the forward shock is now moving through a much denser medium. Although the forward shock accelerates again as it breaks out of the shell and runs down a steep density gradient, it never recovers its original velocity, as is true for the reverse shock. The forward shock interaction does become nearly adiabatic again (see Section 4), so the velocity remains higher than during the collision with the shell. By this time, the shell has gained substantial mass through sweeping up the surrounding medium. Therefore its forward momentum is high, and the velocity remains nearly constant for a long period of time because the outer wind has insufficient mass to decelerate it.

The abrupt loss of forward velocity in the reverse shock shell is, in principle, a robust characteristic of SN–shell interaction. Whether or not it is actually observable, however, is unclear. If the density of the pre-shock CSM is high, as it needs to be in the case of the more luminous SNe IIn, then one might expect the pre-shock gas to be very optically thick (Smith & McCray 2007; Smith et al. 2010) and the emitting surface may be well outside the shock. In that case, the observed Hα line profile would be dominated by the narrow component from photoionized pre-shock gas (typically a few 10^2 km s^{-1}) and broad electron scattering wings (e.g. Chugai 2001; Dessart et al. 2009) out to a few 10^3 km s^{-1}. This is indeed thought to be the case for SN 2006gy, as discussed in detail by Smith et al. (2010).

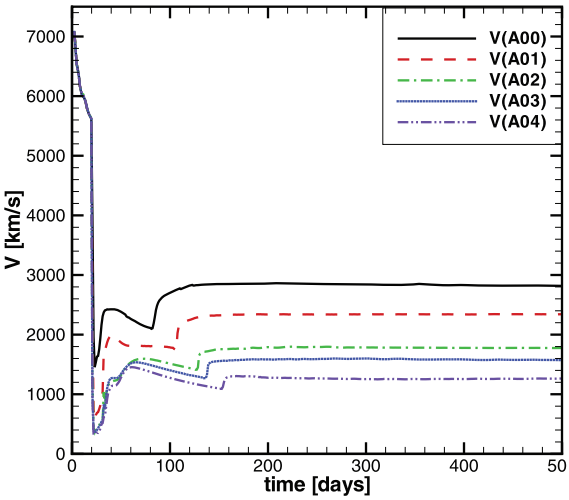

Figure 19. Shocked gas velocities for the same simulations as in Fig. 11. The velocity drops very abruptly when the SN hits the circumstellar shell, then rises again as the SN plows through the gas, then rises once more as it breaks out and makes the transition from a radiative shock back to an adiabatic one. The final velocity depends clearly on the mass of the shell.

The *final* shocked gas velocity, on the other hand, should be easily observable in all cases because of lower optical depths at larger radii and at late times, and may therefore provide an unambiguous constraint on the CSM mass and SN energy. In Fig. 19, which shows the velocity for the same simulations as Fig. 11, we can see that the final velocity does in fact depend strongly on the mass of the circumstellar shell. If the shell mass is relatively high, the velocity decreases by a larger amount as momentum is conserved.

In Fig. 20, we show the shocked gas velocity for the same simulations as Fig. 12. This demonstrates the effect of the wind velocity and mass-loss rate on the shocked gas velocity. As all SNe have the same total energy in these simulations, the higher mass SNe start out with lower velocity. As can be seen, the mass-loss rate only matters in the initial stage, before the collision between the SN and the circumstellar shell. The wind velocity does make a significant difference as it determines the location of the shell relative to the star and therefore the timetable of the interactions, but it does not strongly influence the final speed of the shocked shell.

In Fig. 21, which shows the reverse shock velocity for the same simulations as Fig. 13, we demonstrate the effect of the mass of the SN ejecta on the reverse shock velocity. As all SNe have the same total energy in these simulations, the higher mass SNe start out with lower velocity. As the ejecta collide with the 10 $M_{\odot}$ shell, the lower mass SNe slow down more, since they have less momentum. Still, after the collision, the lowest mass SN is still moving with the highest velocity and is the first to break out of the circumstellar shell.

Finally, Fig. 22 shows the reverse shock velocities for SNe with the same mass, but different total energy. The high-energy SNe start out with higher velocities, but also lose more energy in the collision. Since the collision takes place at an earlier stage, they slow down more, so the final difference in velocities is much less than initially. However, the total SN kinetic energy is perhaps the most influential factor in determining the final shell speed.

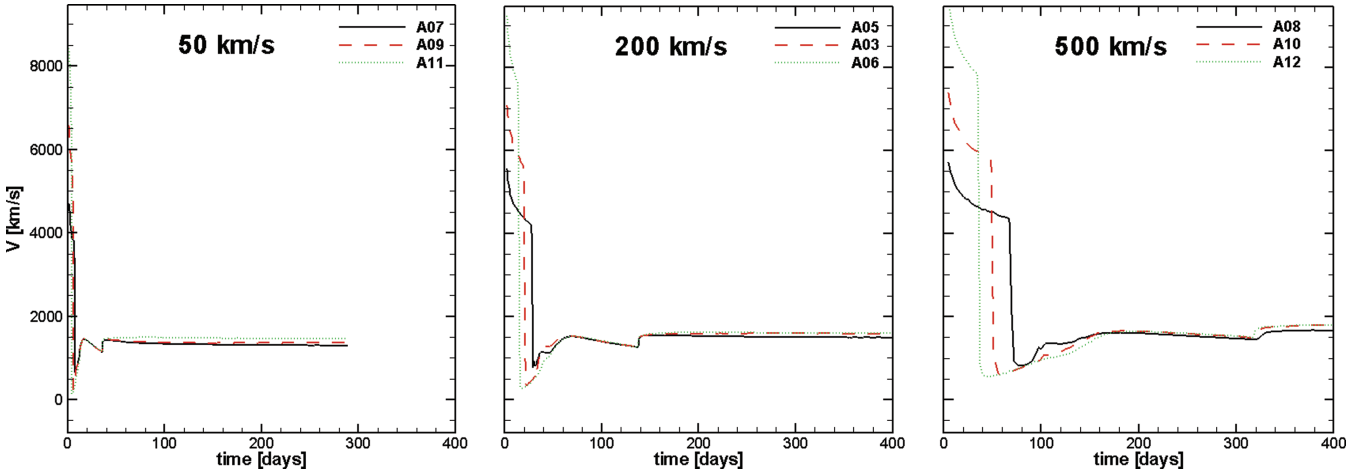

Figure 20. Shocked gas velocities for the same simulations as in Fig. 12. The wind velocity changes the entire shape of the light curve, as it changes the location of the shell, whereas the wind mass loss rate is only important in the initial stages.

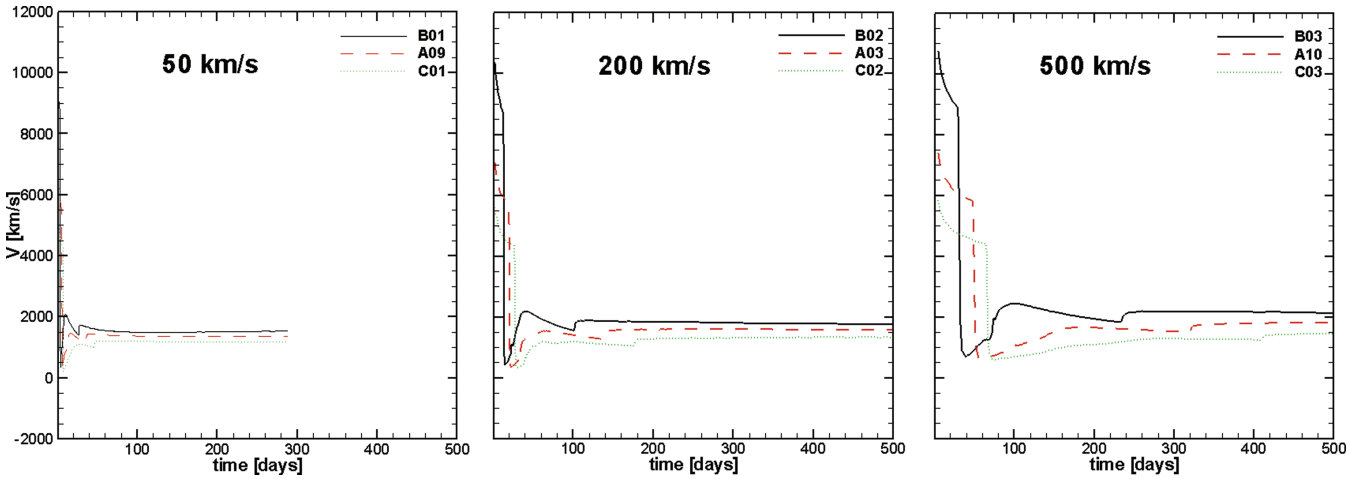

Figure 21. Shocked gas velocities for the same simulations as in Fig. 13. The high-mass SNe, which have relatively low velocity, slow down less than the low-mass SNe, but not enough to reverse the shock velocities.

Because of the specific nature of the collision, there are several different features that can determine the observed shock velocity of the SN. To illustrate this effect, we show three alternative velocity curves in Fig. 23, all based on simulation A03. (A) The velocity of the reverse shock, (B) the velocity of the gas that has passed through the reverse shock and (C) the velocity of the shocked gas that has the highest density. Initially, all three curves move together. The gas flow of shocked gas is slightly faster than the reverse shock itself, since this gas is actually moving through the shock. Before the collision with the circumstellar shell, the highest density of shocked gas is at the reverse shock, since this is where the SN ejecta piles up. This changes once the SN collides with the shell. The reverse shock recoils from the collision, stopping completely or even reversing, depending on the density of the shell. The gas velocity inside the shock decreases as well, but not as much, since this is governed by the shock conditions. The shock changes from adiabatic to isothermal, restricting the velocity jump over the shock. As the SN then ploughs through the shell, the location of the highest density feature changes. It is no longer at the reverse shock, but rather at the forward shock, where gas from the shell is being swept up. Therefore, the flow speed of the high-density feature actually becomes lower than the velocity of the reverse shock, since we are now sampling gas that is still in the process of being accelerated. Once the blast wave breaks out of the shell, the original situation is recreated, as once more the highest density occurs at the reverse shock and the shock conditions change back from isothermal to adiabatic.

Examining Figs 19 through 23, one can see that velocities measured in spectra obtained at early times can be powerful diagnostics of the rapid changes occurring during the initial shell collision, while later spectra that provide estimates of the final coasting velocity of the CDS *are key diagnostics of the energy and momentum budget of the explosion*. A potential complication for the early-time velocities, especially with more luminous SNe IIn, may arise if the inner CSM is very optically thick. If the CSM outside the shock is highly opaque, then a radiative precursor may cause the photosphere to reside outside the shock (Smith et al. 2010), in which case the observed velocities are not indicative of the true expansion

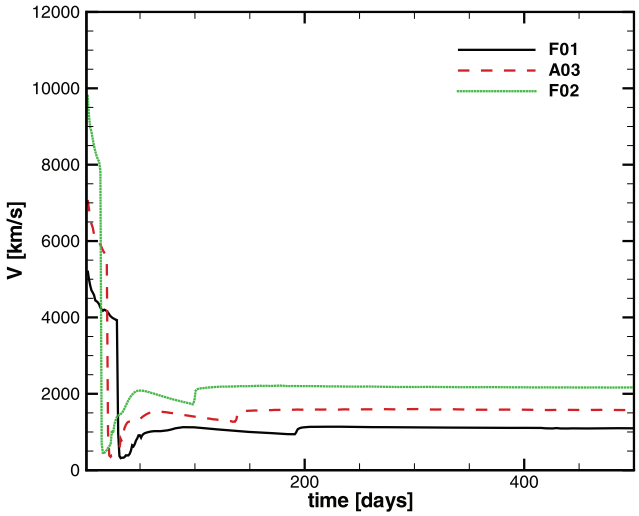

Figure 22. Reverse shock velocities for the same simulations as in Fig. 15, illustrating the effect of SN energy on $v(t)$. The more rapid deceleration of F02 occurs simply because the fastest ejecta reach the inner boundary of the dense CSM shell sooner. The higher energy SN has higher speeds at later phases during the collision.

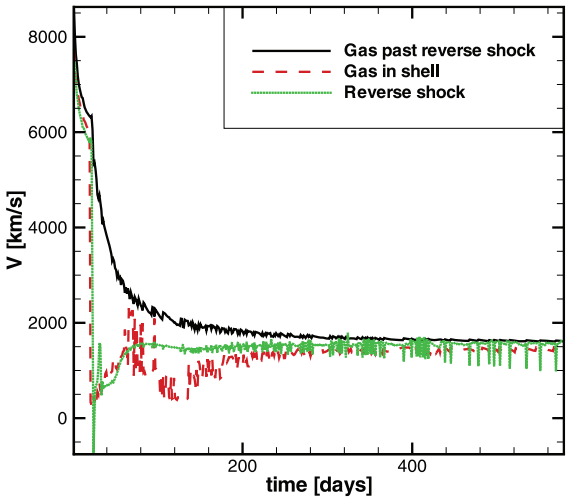

Figure 23. Velocity curves for the reverse shock, shocked gas flow past the reverse shock and highest density shocked gas (the shell) for simulation A03.

speed. In any case, combinations of photometry and spectra at early times while the SN is still on the rise to peak are quite valuable in breaking the degeneracy of various models.

7 DISCUSSION

7.1 The influence of SN and shell properties

In the previous sections, we have shown how circumstellar shells can influence the evolution of both the observed SN light curve and the observed velocity. The presence of a substantially dense circumstellar shell always causes an increase in the radiative luminosity, lasting until the blast wave breaks through the shell. The height of this luminosity peak depends primarily on the density of the shell (and so, also on its total mass and speed), in the sense that denser shells invariably lead to higher luminosities for the same underlying SNe. The duration of the luminosity peak is a direct consequence of the time it takes the blast wave to propagate though the shell, so it depends on the total mass of the shell, its expansion speed, and its inner and outer radii (i.e. the *duration* of the pre-SN ejection episode). A relatively more massive shell produces a slower blast wave, increasing the duration of the light curve peak and causing a higher luminosity. A faster expansion speed for the shell will also stretch the duration of the light curve peak by increasing its outer radius, but will make it less luminous for the same mass.

In our simulations, typical luminosity peaks for spherical shells tend to have a flat plateau, which is either horizontal, or angled downwards as the shock velocity decreases over time. The beginning and end of the light curve peaks are clearly defined with sharp edges, but this is just a result of our simplifying assumption that the shell has sharp inner and outer boundaries; real shells may have more complicated density profiles. These characteristics tend to disappear if the nebula is bipolar in shape, because different latitudes in the bipolar shell are hit by the blast wave at different times, and so the light curve shape is smoother.

Whereas the total luminosity and the visual luminosity peak when the blast wave collides with the circumstellar shell, the temperature of the emitting gas decreases as the shock slows. A gradual decline in the characteristic temperature inferred from the continuum slope in visual-wavelength spectra or multi-band photometry has been seen in several well-studied examples of very luminous SNe IIn, such as SN 2005gj, SN 2006gy and SN 2006tf (Prieto et al. 2007; Smith et al. 2008a, 2010). The X-ray drop may not be observed if initial phases are optically thick and X-rays are fully absorbed and reprocessed. Trapping at high optical depths is an effect that we have not included directly in our simulations; we consider it likely, therefore, that the visual radiation will trace the bolometric luminosity at early times, as we discussed earlier. This is why we have shown the bolometric luminosity light curve in our plots. Luminosity at high energies increases again once the SN breaks out of the shell and interacts with the (relatively) low-density wind outside the shell. This change in shock temperature is less clearly defined if the shell is bipolar, because both high- and low-velocity interactions can occur simultaneously in different parts of the shell. A clumpy CSM may produce a similar effect.

The observed velocity evolution of the dense post-shock H shell depends strongly on the CSM density and SN energy in our simulations. This velocity decreases steeply in the earliest phase of the expansion when the blast wave sweeps through the wind inside the dense CSM shell, and then it takes another drop when the shock hits the circumstellar shell. However, these velocities in the earliest phases may be difficult to observe because of high optical depth effects that are not taken into account in our simulations, as noted above for the early light curve shape. The characteristic velocity observed *after* the SN/shell collision ends depends on the shell mass, SN mass and the total explosion energy, and is typically 1–3 $\times$ 10^3 km s^{-1} in our simulations. This is comparable to the observed linewidths in luminous SNe IIn like SN 2006tf (Smith et al. 2008a) or SN 2005gj (Prieto et al. 2007). The faster speeds of $\sim$4000 km s^{-1} in SN 2006gy (Smith et al. 2010) imply a higher energy explosion and a relatively high-mass SN. Indeed, Smith et al. (2010) estimated an explosion energy of at least 5 $\times$ 10^{51} erg for SN 2006gy.

The mass and initial speed of SN ejecta (and hence, the total explosion energy) also influence the evolution of the velocity. SNe with higher ejecta mass have higher inertia and are decelerated less, but they also have slower initial expansion speeds for explosions

assumed to have the same total kinetic energy, and so they can end up with slower final expansion speeds. A more energetic and relatively more massive SN explosion will emerge from the shell collision episode with a faster final shock speed. Since there is some degeneracy in any one type of observed property, spectral observations of the pre-shock CSM speed, the post-shock shell and the SN ejecta speeds (if they can be seen) are valuable to combine with estimates of the luminosity from photometry to derive the physical properties of the CSM interaction.

7.2 The shock conversion efficiency

Since some very luminous SNe IIn have measured values for their total radiated energy approaching or even exceeding the canonical SN explosion kinetic energy of 10^{51} erg, the efficiency at which they convert some fraction of their initial kinetic energy into post-shock thermal energy and then radiation is the key. In the shell-shocked model (Smith & McCray 2007), high efficiencies are allowable because of the large radius at which shock energy is thermalized, allowing the SN to radiate before it expands and loses that thermal energy adiabatically. The second to last column of Table 1 lists the efficiency of this conversion as the ratio of the total energy lost via radiation in each simulation to the initial explosion kinetic energy of the SN, or $dE/E_{\rm SN}$. In Fig. 24 we plot this efficiency as a function of another ratio, which is the CSM shell mass compared to the total mass in both the SN ejecta and CSM. We show the results for several simulations to demonstrate various trends.

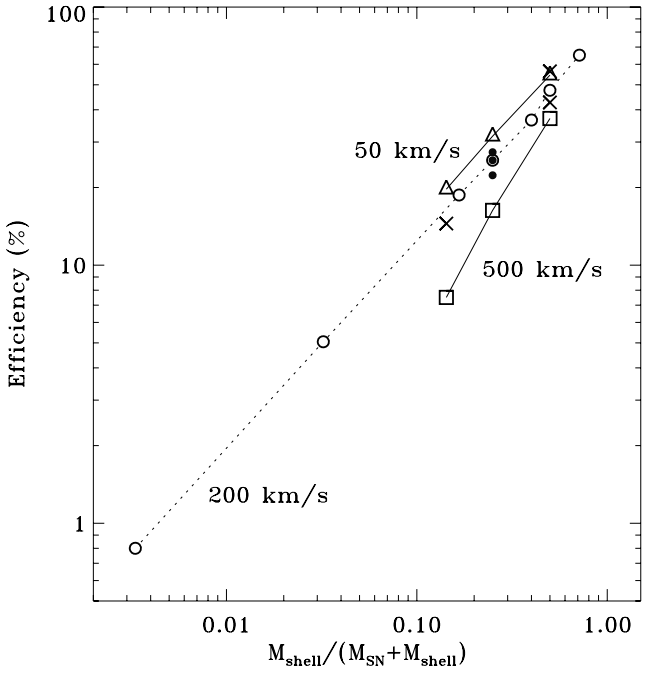

Figure 24. The total efficiency (per cent) in converting shock kinetic energy into radiated energy from Table 1 for several representative simulations, plotted as a function of the ratio of CSM shell mass to the total mass involved (SN ejecta + shell). The unfilled circles (and dotted line) represent our baseline simulations with SN ejecta with 10^{51} erg running into 200 km s^{-1} shells of various masses ('A' models, plus B02 and B04). The unfilled triangles and squares are similar but for CSM speeds of 50 and 500 km s^{-1}, respectively. The filled circles are models F01, A03 and F02, showing the effect of different explosion energy for the same shell parameters. The Xs show models G01, H01 and C01 (all with $V_{\rm exp}$ = 200 km s^{-1}), special cases that have extended CSM mass or lower-mass SN ejecta.

The basic result is that efficient conversion of SN kinetic energy into radiation via CSM interaction requires a CSM mass that is comparable to or larger than the mass of the SN ejecta. The primary criterion for luminous SNe IIn that result from core-collapse SNe is therefore the presence of several $M_\odot$ of circumstellar gas which must have been ejected very shortly before the SN. Explosions of very massive stars can have CSM interaction that is not very luminous if the CSM mass is small compared to the SN ejecta mass (as long as the SN ejecta are slow and heavy for a standard energy). A very effective way to convert a larger fraction of the total initial energy (more than half) into radiation is to have a more extended CSM shell at the same density, as in simulation B04, tracing mass loss for a longer time prior to the SN explosion. Of course, the longer a simulation runs into CSM material, the more kinetic energy can be converted into light – if one waits for ∼100 yr or more, an extended SN remnant can tap a significant fraction of the total energy. Our aim here, however, is to study objects that do this very quickly in ∼1 yr and thereby produce high luminosities during the initial light-curve peak.

The pre-shock CSM speed also has some minor effect on the efficiency, in the sense that slower CSM speeds lead to denser environments that trap more of the available kinetic energy because of their denser post-shock gas, and consequently, more efficient cooling. Also mildly influential is the speed of the SN ejecta, or equivalently, the SN explosion kinetic energy. More energetic explosions are more efficient in converting their available energy reservoir to radiation due to the higher velocity drop at the reverse shock. Thus, mild increases in explosion energy offer an alternative to exceedingly massive CSM shells in order to produce very luminous SNe IIn. Again, however, the CSM must be extended and massive in order to maintain that high luminosity for an extended time.

7.3 Comparisons to observations of luminous SNe IIn

The central motivation for this study was to explore shock interaction with dense pre-SN CSM shells as a possible engine for the visual light from the emerging class of extremely luminous SNe, and to ask whether observed light curves can be compared to expectations of hydrodynamic simulations in order to constrain the physical properties of those shells and the underlying SNe. Below we briefly mention two recent well-observed examples that have been our primary objects for comparison: (1) SN 2006gy (Smith et al. 2007; Ofek et al. 2007) was the first of these super-luminous SNe that raised many questions about our understanding of the power sources for these objects and about massive star evolution, and (2) SN 2006tf (Smith et al. 2008a) which was nearly as luminous. Both have optical spectra of Type IIn suggesting the presence of dense CSM, although SN 2006tf appears to fit the canonical picture of CSM interaction as the power source with fewer complications (Smith et al. 2008a). Both appear to have high optical depths at early phases. The energy sources for these two SNe are of particular interest because, unlike more common SNe IIn at lower luminosity, their total radiated energy severely taxes the total SN energy budget: the energy radiated in visual light was 0.7×10^{51} erg for SN 2006tf (Smith et al. 2008a) and 1.6×10^{51} erg for SN 2006gy (Smith et al. 2007). Making a bolometric correction based on the observed temperature yields $E_{\rm rad} \simeq 2.5 \times 10^{51}$ erg for SN 2006gy, and including the kinetic energy remaining in the shell pushes the total initial explosion energy to at least 5×10^{51} erg (Smith et al.

2010). For SN 2006gy, a pair instability SN or diffusion from an opaque shocked shell have also been suggested as possibilities for powering the observed luminosity (Smith & McCray 2007; Smith et al. 2007; Ofek et al. 2007; Woosley et al. 2007), although detailed analysis of its spectral evolution favours the opaque shocked shell model (Smith et al. 2010).

Two other SNe, SN 2005ap (Quimby et al. 2007) and SN 2008es (Miller et al. 2009; Gezari et al. 2009), have also been discovered recently to be among the most luminous SNe known. In fact, their peak luminosities are somewhat higher than SN 2006gy, although they faded more quickly. We do not consider these for direct comparison with the same type of model discussed here because their spectra are not of Type IIn, but rather, they had normal broad lines in their spectra indicating a photosphere receding through fast ejecta. The lack of narrow emission lines makes it likely that their radiation is produced primarily by diffusion from an opaque shocked envelope, as in the model of Smith & McCray (2007), but with a smaller envelope mass than for SN 2006gy. The parameters in some of our simulations with slower (and therefore more denser) CSM and higher conversion efficiencies, such as B01, might be appropriate for these objects if diffusion were properly accounted for. Alternatively, it has recently been suggested that these SNe may be powered by the birth of magnetars (Kasen & Bildsten 2010; Woosley 2009), energizing the opaque SN ejecta from within.

We did not tune models specifically to fit the observed light curves of SNe 2006gy and 2006tf, but we did explore a range of parameters for combinations of SNe and CSM shells comparable to relevant parameters estimated from observations (Ofek et al. 2007; Smith et al. 2007, 2008a, 2010; Woosley et al. 2007). Among our models, some of the highest peak luminosities were attained with relatively low mass (and therefore fast) SNe running into slower CSM shells, such as B01 and B02 (10 $M_\odot$ SNe), or A07, A09 and A11 (slower 50 km s^{-1}shells). Although these models achieved very high peak luminosities comparable to those of the most luminous observed SNe IIn, they faded too quickly, and so they fall far short of achieving the duration and total radiated light output of events like SNe 2006gy and 2006tf. Lower mass SNe run out of momentum too quickly, or overrun the compact CSM shells too quickly. These low- and moderate-mass models may be applicable to SNe 2005ap and 2008es, which attained high peak luminosities and faded quickly as mentioned above. Again, an important consideration is that our models do not include the possible delayed effects of diffusion when high optical depths are important, as one might expect for massive and slow (and therefore dense) CSM shells (Smith & McCray 2007). Including this may produce a smoother light curve (Falk & Arnett 1977), especially in the sense that it would dampen and round-out the sharp initial peak in many of our simulations. Thus, it is possible that models such as B01 could be dominated by diffusion and may not appear as SNe of Type IIn, but confirming this conjecture requires additional work beyond the scope of this paper. Diffusion through an opaque shell, however, would not alter the later phases of our light curves after maximum light.

There were some models that came close to matching the light-curve behaviour of SNe 2006gy and 2006tf with both high luminosity and relatively long durations. These were models with SNe that had very massive and extended shells of 10–25 $M_\odot$, although even these seemed somewhat insufficient. Fig. 25 compares the observed light curves of these two SNe (data from Smith et al. 2007, 2008a) to models A04, B02 and B04. All of these have shell expansion speeds of 200 km s^{-1}, close to the observed values of pre-shock material for SNe 2006tf and 2006gy (Smith et al. 2007, 2008a).

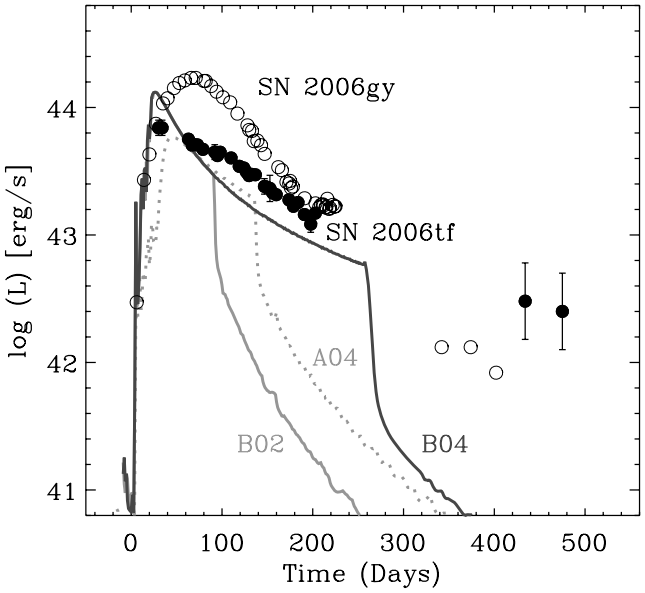

Figure 25. This plot compares a few selected models to light curves of the two most luminous SNe IIn known. SN 2006gy (data from Smith et al. 2007, 2008c) is shown with unfilled circles, and SN 2006tf (Smith et al. 2008a) is shows with filled circles. The models are A04 (30 $M_\odot$ SN and 20 $M_\odot$ shell; dotted grey), B02 (10 $M_\odot$ SN and 10 $M_\odot$ shell; solid grey) and B04 (10 $M_\odot$ SN and 25 $M_\odot$ shell; dark grey). Model B04 is the same as B02 except that the shell has a larger outer radius (it is thicker at the same density) and therefore has a larger total mass. While these models may account for the peak luminosities of SN 2006tf, they fall short of the peak luminosity for SN 2006gy and fade too quickly for both. It is likely that simulations with more extended and more massive CSM shells or more energetic SNe need to be explored in these two particular cases. The very late time data at around 400 d for SN 2006gy may have some contribution from a light echo (e.g. Smith et al. 2008c), but the late-time luminosity after 1 yr for SN 2006tf is dominated by strong ongoing CSM interaction because strong Hα emission is seen in the late-time spectrum (Smith et al. 2008a). For a typical Type IIp light curve, see Figs 10 and 11.

7.3.1 SN 2006tf

The light curve of SN 2006tf shows a slow and steady decline from peak luminosity, the approximate rate of which is reproduced in all three models shown. In our simulations, this decline rate is mainly due to the deceleration of the post-shock gas as the SN ejecta sacrifice energy to radiation. An interesting result is that this decline rate during the main light curve peak for model B04 roughly matches the radioactive decay rate of ^{56}Co, even though there is no luminosity from radioactivity included in these simulations – in other words, luminosity from shock–CSM interaction alone can in some cases mimic the radioactive decay rate. (One might also expect a similar decline from a steeper density gradient in the CSM shell, or a different velocity/density law in the SN ejecta. In SN 2006gy, for example, recent evidence points to a Hubble-like expansion law in the CSM (Smith et al. 2010). However, none of the models sustains the high luminosity for a long-enough time. SN 2006tf shows relatively high luminosity above 10^{42} erg s^{-1} even at very late times, *more than 1 yr after peak*, consistent with a continuation of the same decay rate, but all three models in Fig. 25 drop long before that time. In our simulations, this drop occurs when the forward shock exits the outer boundary of the dense shell and continues into the lower-density exterior wind shed by the star before it ejected the CSM shell. A similar drop in luminosity was observed in the

light curve of SN 1994W, and was also attributed to the shock overrunning the outer boundary of a CSM shell (Chugai et al. 2004). This sharp drop is not usually seen in the light curves of SNe IIn, however, suggesting that most SNe IIn have more extended CSM shells.

We explored the effect that changing the outer shell boundary has on the light curves. Models B02 and B04, both shown in Fig. 25, are identical up to the point when the radius of the outer shell boundary is reached in model B02. At this time, occurring around day 100, the luminosity in model B02 plummets as the shock runs out of dense CSM to interact with. In model B04, however, we simply continued the same shell properties to a larger radius by having the shell ejection occur with the same mass-loss rate over a longer time interval (Δt = 5yr instead of 2 yr, both ending 2 yr before core collapse). Thus, the slow decline from peak luminosity continued at roughly the same rate until day ∼260, when its forward shock reached the outer shell boundary and the luminosity finally plummeted. This larger outer radius required a much larger shell mass, increased from 10 $M_\odot$ in model B02 to 25 $M_\odot$ in model B04. The general shape and luminosity of model B04 are similar to the 25 $M_\odot$ shell model that Woosley et al. (2007) suggested for SN 2006gy, although Smith et al. (2008a) noted that it also fits the early light curve of SN 2006tf well. A shell mass of 25 $M_\odot$ is near the limit of what one might believe from a non-terminal stellar outburst if giant eruptions of LBVs like η Carinae are representative (Smith et al. 2003; Smith & Ferland 2007). Shell masses beyond 25 $M_\odot$ also begin to press the most basic limitations of even a very massive star's mass budget at the end of its life (see e.g. Smith & Owocki 2006).

However, even the extremely massive shell of 25 $M_\odot$ in model B04 cannot sustain a high luminosity long enough to account for the +1 yr observations of SN 2006tf (Fig. 25) because it drops too soon. Instead, the late-time luminosity of SN 2006tf seems to continue the same slow decline rate. The corresponding CSM shell mass that this would imply (roughly 50 $M_\odot$) is staggering if the continued high luminosity were the result of simply extending the same shell to larger radii. One way to avoid such implausibly high shell mass would be to lower the density of the envelope but increase the total SN explosion energy above 10^{51} erg. Higher explosion energy leads to faster SN ejecta speed, so consequently, higher instantaneous luminosity can be achieved with lower shell densities. A larger explosion energy also relieves some of the strain on the efficiency of converting kinetic energy into light, since the total radiated energy of SN 2006tf is almost 10^{51} erg.

7.3.2 SN 2006gy

This SN presents additional challenges, since the total radiated energy actually exceeded 10^{51} erg (Smith et al. 2007, 2010), requiring a more energetic SN explosion no matter what the CSM properties are. None of our models were able to achieve the combination of the high peak luminosity and long duration of SN 2006gy, although our most energetic SN explosion was only 2×10^{51} erg. Following the above arguments for SN 2006tf, then, one might expect that models with a more energetic explosion could match the light curve of SN 2006gy without having implausibly high CSM mass (Woosley et al. 2007). For example, the smooth light curve shape and slow rise to maximum are traits that were seen in our simulations with bipolar CSM shells, so one can imagine that a set of parameters similar to model D02 but with higher explosion energy may account for the light curve of SN 2006gy. This will be explored in a future paper. Diffusion from opaque shocked shell may also lead to a smooth light curve appropriate for SN 2006gy (Smith & McCray 2007), and we have not included these high optical depth effects in our simulations.

8 CONCLUSION

In this paper we describe the influence of massive circumstellar shells on core-collapse SN light curves, with the primary motivation of trying to understand the power source of extremely luminous Type IIn events and their relation to the diverse population of SNe IIn. We show how these circumstellar shells can indeed create extreme peaks in the luminosity such as have been observed in Type IIn SNe like SN2006gy and SN2006tf. The luminosity of these SNe would require extreme amounts of ^{56}Ni if they are powered by radioactive decay, but if interactions in the CSM provide the power instead, then the shell masses and speeds that are required have reasonable precedent from observed properties of spatially resolved shells around nearby massive stars (see Smith & Owocki 2006 and references therein).

Our investigation is by no means exhaustive. Pre-SN circumstellar shells may have a wide range of masses, expansion speeds and radii, whereas we have adopted simplified shell geometries for illustrative examples. Additionally, the underlying SNe ejecta may have wide diversity in explosion energy, mass and ejecta speed. In this preliminary investigation, our approach has been to vary each of these parameters individually to illustrate their influence on the light curve rather than attempting to accurately model any individual SN. We have attempted to find general ways to distinguish between different kinds of shells, using trends in the observed shapes of the light curves, their characteristic emission temperature and observed shock speeds. We find that observations of the evolution of the shock speed is necessary to help break the degeneracy in the other free parameters, while observations of the speed of the pre-shock CSM help considerably as well (see e.g. Salamanca et al. 2002; Smith et al. 2007, 2008a, 2009, 2010; Trundle et al. 2008). This can be used to analyse the mass-loss history of massive stars in the last years prior to the explosion, which can be a powerful tool for studying the final stages of stellar evolution. Ultimately, we wish to know the physical origin of these SN-precursor events.

The key result is that we confirm the large masses of circumstellar shells hypothesized to account for some recent luminous SNe IIn (Smith & McCray 2007; Smith et al. 2007, 2008a, 2010; Woosley et al. 2007), as well as the high mass and explosion energy of the underlying SNe. One can also produce a very high peak luminosity with lower mass if the shell is slow and the SN ejecta are fast, but a lower mass shell cannot yield both a high peak luminosity and a long duration of $\gtrsim$100 d seen in some luminous SNe IIn. In fact, we suspect that even larger shell masses or larger explosion energies are needed to account for the observed light curves of the most luminous SNe IIn. Thus, more detailed attempts to model individual objects will be the focus of a second paper in this series.

8.1 Future developments

Further research is required for quantitative analyses of observed SN IIn light curves and to extract reliable absolute values of shell masses and SN explosion energies. This must include adding the luminosity contribution from the underlying SN photosphere (powered by diffusion or radioactive decay) in cases where the CSM interaction luminosity is not extremely high compared to the ejecta photosphere, as well as using an improved treatment of post-shock

cooling and radiative transfer at high optical depths in order to more accurately model the emergent radiation from the post-shock shells in these simulations. As noted by Smith & McCray (2007) and Smith et al. (2008a, 2010), it is likely that the CSM will be highly opaque, especially at the earliest phases, so the effects of radiative diffusion should be taken into account to properly model the emergent luminosity. Finally, all our simulations have adopted a Type II-P core-collapse SN density profile, but other types of SNe with different density profiles need to be investigated in a similar manner, since any type of SN can, in principle, be a Type IIn event if it runs into a dense H-rich environment.

ACKNOWLEDGMENTS

AJM acknowledges support from NSF grant AST-0507581, from the FWO, grant G.0277.08, and K.U.Leuven GOA/09/009. NS was partially supported by NASA through grants GO-10241 and GO-10475 from the Space Telescope Science Institute, which is operated by AURA, Inc., under NASA contract NAS5-26555, and through Spitzer grants 1264318 and 30348 administered by JPL. We thank R.H.D. Townsend for the use of his radiative cooling module. AJM thanks G. García-Segura, N. Langer and R. Kotak for helpful discussion. We also thank our anonymous referee for his insightful comments, which helped us to improve out paper.

REFERENCES

Aretxaga I., Benetti S., Terlevich R. J., Fabian A. C., Cappellaro E., Turatto M., della Valle M., 1999, MNRAS, 309, 343
Arnett D., 1996, Supernovae and Nucleosynthesis: An Investigation of the History of Matter from the Big Bang to the Present, Princeton Series in Astrophysics. Princeton University Press, NJ
Chevalier R. A., 1977, ARA&A, 15, 175
Chevalier R. A., 2005, ApJ, 619, 839
Chevalier R. A., Fransson C., 1992, ApJ, 395, 540
Chevalier R. A., Fransson C., 2008, ApJ, 683, L135
Chevalier R. A., Oishi J., 2003, ApJ, 593, L23
Chugai N. N., 2001, MNRAS, 326, 1448
Chugai N. N., Danziger I. J., 1994, MNRAS, 268, 173
Chugai N. N. et al., 2004, MNRAS, 352, 1213
Clark D. A., 1996, ApJ, 457, 291
Davidson K., Humphreys R. M., 1997, ARA&A, 35, 1
Dessart L., Hillier D. J., Gezari S., Basa S., Matheson T., 2009, MNRAS, 394, 21
Dwarkadas V. V., Owocki S. P., 2002, ApJ, 581, 1337
Dyson J. E., Williams D. A., 1997, The Physics of the Interstellar Medium. Institute of Physics publishing, Bristol, UK
Falk S., Arnett D. W., 1977, ApJS, 33, 515
Filippenko A. V., 1997, ARA&A, 35, 309
Fransson C. et al., 2002, ApJ, 572, 350
Fox O. et al., 2009, ApJ, 691, 650
Gal-Yam A., Leonard D. C., 2009, Nat, 458, 865
Germany L. M., Reiss D. J., Sadler E. M., Schmidt B. P., Stubbs C. W., 2000, ApJ, 533, 320
Gezari S. et al., 2009, ApJ, 690, 1313
Hamuy M., 2003, ApJ, 582, 905
Hillier D. J., Davidson K., Ishibashi K., Gull T., 2001, ApJ, 553, 837
Kasen D., Bildsten L., 2010, ApJ, 717, 245
Kasen D., Woosley S. E., 2009, ApJ, 703, 2205
Leonard D. C. et al., 2002, PASP, 114, 35L
MacDonald J., Bailey M. E., 1981, MNRAS, 197, 995
Matzner C. D., McKee C. F., 1999, ApJ, 510, 379
Miller A. A. et al., 2009, ApJ, 690, 1303
Montes M. J., Van Dyk S. D., Weiler K. W., Sramek R. A., Panagia N., 1998, ApJ, 506, 874
Ofek E. O. et al., 2007, ApJ, 659, L13
Owocki S. P., 2005, Humphreys R. and Stanek K. eds. ASP Conf. Ser. Vol. 332. The Fate of the Most Massive Stars, Proceedings of the Conference held 23–28 May, 2004 in Grand Teton National Park, Wyoming. Astron. Soc. Pac., San Francisco, p. 171
Owocki S. P., Cohen D. H., 2007, ApJ, 648, 565
Owocki S. P., Gayley K. G., Shaviv N. J., 2004, ApJ, 616, 525
Prieto J. L. et al., 2007, preprint (arXiv:0706.4088)
Quimby R. M., Aldering G., Wheeler J. C., Höflich P., Akerlof C. W., Rykoff E. S., 2007, ApJ, 668, L99
Salamanca I., Terlevich R. J., Tenorio-Tagle G., 2002, MNRAS, 330, 844
Schlegel E. M., 1990, MNRAS, 244, 269
Smith N., 2005, MNRAS, 357, 1330
Smith N., 2006, ApJ, 644, 1151
Smith N., Ferland G., 2007, ApJ, 655, 911
Smith N., Hartigan P., 2006, ApJ, 638, 1045
Smith N., McCray R., 2007, ApJ, 671, L17
Smith N., Owocki S. P., 2006, ApJ, 645, L45
Smith N., Townsend R. H. D., 2007, ApJ, 666, 967
Smith N., Gehrz R. D., Hinz P. M., Hoffmann W. F., Hora J. L., Mamajek E. E., Meyer M. R., 2003, AJ, 125, 1458
Smith N. et al., 2007, ApJ, 666, 1116
Smith N., Chornock R., Li W., Ganeshalingam M., Silverman J. M., Foley R. J., Filippenko A. V., Barth A. J., 2008a, ApJ, 686, 467
Smith N., Foley R. J., Filippenko A. V., 2008b, ApJ, 680, 568
Smith N. et al., 2008c, ApJ, 686, 485
Smith N. et al., 2009, ApJ, 695, 1334
Smith N., Chronock R., Silverman J. M., Filippenko A. V., Foley R. J., 2010, ApJ, 709, 856
Stone J. M., Norman M. L., 1992, ApJ, 80, 753
Townsend R. H. D., 2009, ApJS, 181, 391
Trundle C., Kotak R., Vink J. S., Meikle W. P. S., 2008, A&A, 483, L47
Turatto M., Cappellaro E., Danziger I. J., Benetti S., Gouiffes C., della Valle M., 1993, MNRAS, 262, 128
Van Dyk S. D., Weiler K. W., Sramek R. A., Panagia N., 1993, ApJ, 419, L69
van Veelen B., Langer N., Vink J., Garcia-Segura G., van Marle A. J., 2009, A&A, 503, 495
Whalen D., van Veelen B., O'shea B. W., Norman M. L., 2008, ApJ, 682, 49
Williams C. L., Panagia N., Van Dyk S. D., Lacey C. K., Weiler K. W., Sramel R. A., 2002, ApJ, 581, 396
Woosley S. E., 2009, in press (arXiv:0911.0698)
Woosley S. E., Blinnikov S., Heger A., 2007, Nat, 450, 390
Young T. R., 2004, ApJ, 617, 1233

APPENDIX A: LUMINOSITY

This Appendix contains a sample of our luminosity tables. The full tables can be found online (see Supporting Information).

Table A1. luminosity values for simulation O01.

Time (s)	log10(L) (erg s^{-1})
1.0000000E+05	4.0854548E+01
2.0000000E+05	4.0681275E+01
3.0000000E+05	4.0674991E+01
4.0000000E+05	4.0714879E+01
5.0000000E+05	4.0557764E+01
6.0000000E+05	4.0541291E+01
7.0000000E+05	4.0630674E+01
8.0000000E+05	4.0439978E+01
9.0000000E+05	4.0538254E+01
1.0000000E+06	4.0346281E+01

Table B1. Shock velocity values for simulation O01.

Time (s)	V(volume averaged) (cm s^{-1})	V (mass averaged) (cm s^{-1})
2.0000000E+05	6.3296810E+08	7.0761081E+08
3.0000000E+05	6.1563164E+08	6.8375272E+08
4.0000000E+05	5.9150803E+08	6.5441661E+08
5.0000000E+05	5.7608001E+08	6.4455979E+08
6.0000000E+05	5.7573592E+08	6.3470001E+08
7.0000000E+05	5.6127737E+08	6.1689406E+08
8.0000000E+05	5.4696696E+08	6.0784766E+08
9.0000000E+05	5.3620586E+08	6.0075791E+08
1.0000000E+06	5.3759244E+08	5.9993685E+08

APPENDIX B: SHOCK VELOCITY

This Appendix contains a sample of our shock velocity tables. The full tables can be found online (see Supporting Information).

SUPPORTING INFORMATION

Additional Supporting Information may be found in the online version of this article:

Appendices A and B. Luminosity and shock velocity.

Please note: Wiley-Blackwell are not responsible for the content or functionality of any supporting materials supplied by the authors. Any queries (other than missing material) should be directed to the corresponding author for the article.

This paper has been typeset from a TEX/LATEX file prepared by the author.